Export fluxes in a naturally iron-fertilized area of the Southern Ocean: importance of diatom spores and faecal pellet for export (part 2).

M. Rembauville[1,2], S. Blain[1,2], L. Armand[3], B. Quéguiner[4] and I. Salter[1,2,5]

[1] Sorbonne Universités, UPMC Univ Paris 06, UMR 7621, LOMIC, Observatoire Océanologique, Banyuls-sur-Mer, France.

[2] CNRS, UMR 7621, LOMIC, Observatoire Océanologique, Banyuls-sur-Mer, France.

[3] Department of Biological Sciences and Climate Futures, Macquarie University, New South Wales, Australia

[4] Aix-Marseille Université, Université de Toulon, CNRS/INSU, IRD, MOI, UM 110, Marseille, France.

[5] Alfred-Wegener-Institute for Polar and Marine research, Bremerhaven, Germany.

Correspondance to : M. Rembauville (rembauville@obs-banyuls.fr).

Abstract

The biological composition of the material exported to a moored sediment trap located under the winter mixed layer of the naturally-fertilized Kerguelen Plateau in the Southern Ocean was studied over an annual cycle. Despite iron availability in spring, the annual particulate organic carbon (POC) export (98.2 mmol m^{-2}) at 289 m was low but annual biogenic silica export was significant (114 mmol m^{-2}). This feature was related to the abundance of empty diatom cells and the ratio of full:empty cells exerted a first order control in BSi:POC export stoichiometry of the biological pump. *Chaetoceros Hyalochaete* spp. and *Thalassiosira antarctica* resting spores were responsible for more than 60 % of the annual POC flux that occurred during two very short export events of <14 days in spring-summer. Relatively low diatom fluxes were observed over the remainder of the year. Faecal pellet contribution to annual carbon flux was low (34 %) and reached its seasonal maximum in

autumn and winter (> 80 %). The seasonal progression of faecal pellet types revealed a clear transition from small spherical shapes (small copepods) in spring, larger cylindrical and ellipsoid shapes in summer (euphausiids and large copepods) and finally large tabular shapes (salps) in autumn and winter. We propose in this High Biomass, Low Export (HBLE) environment that small, highly silicified, fast-sinking resting spores are able to bypass the intense grazing pressure and efficient carbon transfer to higher trophic levels that are responsible for the low fluxes observed the during the remainder of the year. More generally our study also provides a statistical framework linking the ecological succession of diatom and zooplankton communities to the seasonality of carbon and silicon export within an iron-fertilized bloom region in the Southern Ocean.

1 Introduction

The Southern Ocean is the place of exposure of old upwelled waters to the atmosphere and the formation of mode waters, thereby ventilating an important part of the global Ocean and playing a central role in distributing heat, carbon and nutrients in the global Ocean (Sarmiento et al., 2004; Takahashi et al., 2012; Sallée et al., 2012). Silicon trapping occurs in the Southern Ocean because silicon is stripped out of the euphotic zone more efficiently than phosphorous and nitrogen (Holzer et al., 2014). It is generally acknowledged that regional variations in plankton community structure are responsible for variations in nutrient stoichiometry in the Southern Ocean (Jin et al., 2006; Weber and Deutsch, 2010) and that the biological pump is a central process regulating this stoichiometry (Ragueneau et al., 2006; Salter et al., 2012; Primeau et al., 2013). These characteristics emphasize the importance of biological processes in the Southern Ocean waters for the availability of silicic acid and nitrate (Sarmiento et al., 2004; Dutkiewicz et al., 2005) as well as phosphate (Primeau et al., 2013) at lower latitudes, thereby regulating part of the productivity of the global Ocean. It has been proposed that change in the uptake ratio of silicate and nitrate by Southern Ocean phytoplankton in response to increased iron availability during the Last Glacial Maximum could have played a substantial role in varying atmospheric CO_2 (Brzezinski et al., 2002; Matsumoto et al., 2002).

Primary production in the Southern Ocean is regulated by macro- and micronutrient availability (Martin et al., 1990; Moore et al., 2001; Nelson et al., 2001; Moore et al., 2013) and light-mixing regime (Venables and Moore, 2010; Blain et al., 2013). The complex interaction of these factors introduces strong spatial heterogeneity in the distribution of primary producer biomass (Arrigo et al., 1998; Thomalla et al., 2011). In particular, High Nutrient, Low Chlorophyll (HNLC) areas in the open ocean contrast strongly with highly productive, naturally fertilized, blooms located downstream of island systems such as the

Keguelen Plateau (Blain et al., 2001, 2007), Crozet Islands (Pollard et al., 2002) and South Georgia (Park et al., 2010; Tarling et al., 2012). The diatom-dominated phytoplankton blooms characteristic of these island systems are the product of multiple environmental conditions favorable for their rapid growth (Quéguiner, 2013), which appear to promote POC export from the mixed layer (Nelson et al., 1995; Buesseler, 1998). However the ecological traits of certain species can impact the BSi:POC export stoichiometry (Crawford, 1995; Salter et al., 2012), and may therefore control the biogeochemical function of a particular region of the Southern Ocean (Smetacek et al., 2004; Assmy et al., 2013)

Among the numerous ecological characteristics of plankton communities, algal aggregation (Jackson et al., 2005; Burd and Jackson, 2009), mesozooplankton faecal pellets (Lampitt et al., 1990; Wilson et al., 2008, 2013), vertical migrations of zooplankton and mesopelagic fish (Jackson and Burd, 2001; Steinberg et al., 2002; Davison et al., 2013), radiolarian faecal pellets (Lampitt et al., 2009), and diatom resting spore formation, (Salter et al., 2012; Rynearson et al., 2013) have all been highlighted as efficient vectors of carbon export out of the surface mixed layer. The challenge in describing the principal ecological processes regulating POC export fluxes is the requirement to have direct access to sinking particles. Many of the processes described occur in the upper layers of the ocean, where circulation can strongly influence the reliability of sediment trap collections (Baker et al., 1988; Buesseler et al., 2007). Short term deployments of free drifting sediment traps can be an efficient solution to minimize the hydrodynamic bias (Buesseler et al., 2000; Lampitt et al., 2008) but spatial and temporal decoupling of production and export needs to be considered (Salter et al., 2007; Rynearson et al., 2013). In regions characterized by relatively weak circulation, moored sediment trap observations in areas of naturally fertilized production can track temporal succession of exported material from long-term (several month) blooms (Westberry et al., 2013). Such an approach can partially resolve how ecological processes in

92 plankton communities regulate POC and biomineral export out of the mixed layer (Salter et
93 al., 2012; Salter et al., 2014), although selective processes during export may modify original
94 surface features

95 The central Kerguelen Plateau is a good environment to study the ecological vectors of
96 export with sediment traps due to the naturally fertilized recurrent bloom (Blain et al., 2007)
97 and shallow bathymetry that breaks the strong Antarctic Circumpolar Current flow (Park et
98 al., 2008, 2014). As reported in the companion paper (Rembauville et al., 2014), annual POC
99 export measured by the sediment trap deployment at 289 m beneath the southeastern iron-
100 fertilized Kerguelen bloom is 98±4 mmol m^{-2} y^{-1}. This downward flux of carbon may account
101 for as little as ~1.5 % of seasonal net community carbon production (6.6±2.2 mol m^{-2},
102 Jouandet et al., 2008) and <2 % of seasonally-integrated POC export estimated at 200 m from
103 a dissolved inorganic carbon budget (5.1 molC m^{-2}, Blain et al., 2007). Although
104 hydrodynamical and biological biases related to the shallow moored sediment trap
105 deployment may partly explain the low POC fluxes we report, independent measurements of
106 low POC fluxes (>300 m) at the same station (Ebersbach and Trull, 2008; Jouandet et al.,
107 2014) are consistent with the hypothesis of an intense flux attenuation below the winter mixed
108 layer. These observations suggest a 'High Biomass, Low Export' (HBLE, Lam and Bishop,
109 2007) status characterizing the productive Kerguelen Plateau. HBLE status appears to be a
110 common feature of other productive sites of the Southern Ocean (Lam and Bishop, 2007;
111 Ebersbach et al., 2011; Lam et al., 2011; Maiti et al., 2013; Cavan et al., 2015). Describing the
112 temporal succession of POC and BSi flux vectors from the Kerguelen Plateau is of interest to
113 increase our understanding of the ecological processes characterizing HBLE environments.

114 Numerous studies have described diatom fluxes from sediment trap records in the
115 Southern Ocean (Leventer and Dunbar, 1987; Fischer et al., 1988; Abelmann and Gersonde,
116 1991; Leventer, 1991; Gersonde and Zielinski, 2000; Fischer et al., 2002; Pilskaln et al.,

2004; Ichinomiya et al., 2008; Salter et al., 2012). Highest diatom fluxes recorded by sediment traps (>10^9 valves m^{-2} d^{-1}) were observed in the Seasonal Ice Zone (SIZ) near Prydz Bay and Adélie Land and were dominated by *Fragilariopsis kerguelensis* and smaller *Fragilariopsis* species such as *Fragilariopsis curta* and *Fragilariopsis cylindrus* (Suzuki et al., 2001; Pilskaln et al., 2004). These high fluxes occured in summer and were associated with the melting of sea ice. Changes in light availability and melt water input appear to establish favorable conditions for the production and export of phytoplankton cells (Romero and Armand, 2010). In the Permanently Open Ocean Zone (POOZ), highest diatom fluxes recorded were two orders of magnitude lower ~10^7 valves m^{-2} d^{-1} (Abelmann and Gersonde, 1991; Salter et al., 2012; Grigorov et al., 2014) and typically represented by *F. kerguelensis* and *Thalassionema nitzschioides*. One notable exception is the naturally iron-fertilized waters downstream of the Crozet Plateau where resting spores of *Eucampia antarctica* var. *antarctica* dominated the diatom export assemblage (Salter et al., 2012).

Other studies have reported faecal pellet contribution to POC fluxes in the Southern Ocean (Dunbar, 1984; Wefer et al., 1988; Wefer et al., 1990; Wefer and Fisher, 1991; Dubischar and Bathmann, 2002; Suzuki et al., 2001,2003; Accornero and Gowing, 2003; Schnack-Schiel and Isla, 2005; Gleiber et al., 2012) with a particular emphasis on shelf environments where faecal pellet contribution to POC flux was typically higher than in the oceanic regions (Wefer et al., 1990; Wefer and Fischer, 1991; Schnack-Schiel and Isla, 2005). In the Ross Sea, a northward decreasing contribution to carbon flux of 59 %, 38 % and 15 % for southern, central and northern areas was reported from 235 m sediment traps deployments (Schnack-Schiel and Isla, 2005). Faecal pellets in the Ross Sea were generally represented by larger shapes with only 2 to 3 % of them present as small spherical or ellipsoid shapes and total faecal pellet flux was slightly higher than 10^3 pellet m^{-2} d^{-1}. High faecal pellet contribution to carbon fluxes (> 90 %) have been observed in the Bransfield Strait and the

142 Marginal Ice Zone of the Scotia Sea, and have been linked to the abundance of the Antarctic
143 krill *Euphausia superba*, resulting in maximum recorded fluxes of >5 × 10^5 pellets m^{-2} d^{-1}
144 (Bodungen, 1986; von Bodungen et al., 1987; Wefer et al., 1988). The strong contribution of
145 krill faecal pellets to carbon flux in the western Antarctic Peninsula was confirmed over
146 several years of observations, with the highest contributions to carbon flux succeeding the
147 phytoplankton bloom in January and February (Gleiber et al., 2012).

148 In the present study, particulate material exported from the mixed layer in the naturally
149 fertilized Permanently Open Ocean Zone (POOZ) of the Kerguelen Plateau is described from
150 an annual sediment trap mooring. To develop our understanding of seasonal variability in the
151 ecological flux vectors and particle biogeochemistry we investigate the link between the
152 chemical (POC, PON, BSi) and biological (diatom species and faecal pellet types)
153 components of exported particles. Furthermore, we advance the limitations of previous studies
154 by explicitly distinguishing full and empty diatom cells in the exported material and thereby
155 determine species-specific roles for carbon and silica export.

156 **2 Materials and methods**

157 As part of the multidisciplinary research program KEOPS2 a moored sediment trap
158 (Technicap PPS3) was deployed at 289 m (seafloor depth: 527 m) at the representative bloom
159 station A3 (50°38.3' S – 72°02.6' E) for a period of 321 days (21 October 2011 to 7
160 September 2012). The sediment trap mooring was located within an iron-fertilized bloom site
161 on the southern part of the Kerguelen Plateau (Blain et al., 2007). The cup rotation dates of
162 the sediment trap are listed in Table 1. Details of sediment trap design, hydrological
163 conditions, sample processing, POC and PON analyses and surface chlorophyll *a* data
164 extraction are described in a companion paper (Rembauville et al., 2014). Comparison with
165 thorium-based estimates of carbon export suggests a trapping efficiency of 15-30 % relative to

166 the proxy, although strong particle flux attenuation between 200 m and the trap depth (289 m)
167 might also contribute to the low fluxes. We therefore interpret our results to accurately reflect
168 the relationships between the biological and geochemical signals of the material caught by the
169 sediment trap, which we acknowledge may not necessarily represent the entire particle export
170 at 289 m.

171 **2.1 Biogenic and lithogenic silicon analyses**

172 For the analysis of biogenic silica (BSi) and lithogenic silica (LSi), 2 to 8 mg of freeze-dried
173 material were weighed (Sartorius precision balance, precision 10^{-4} g) and placed into falcon
174 tubes. The extraction of silicon from biogenic and lithogenic particle phases was performed
175 following the Ragueneau et al. (2005) triple NaOH/HF extraction procedure. Silicic acid
176 ($Si(OH)_4$) resulting from NaOH extractions was measured automatically on a Skalar 5100
177 autoanalyzer whereas $Si(OH)_4$ resulting from HF extraction was measured manually on a
178 Milton Roy Spectronic 401 spectrophotometer. $Si(OH)_4$ analyses were performed
179 colorimetrically following Aminot and Kerouel (2007). Standards for the analysis of samples
180 from the HF extraction were prepared in an HF/H_3BO_4 matrix, ensuring the use of an
181 appropriate calibration factor that differs from Milli-Q water. The contribution of LSi to the
182 first leaching was determined by using Si:Al ratios from a second leaching step (Ragueneau et
183 al., 2005). Aluminum concentrations were measured by spectrophotometry (Howard et al.,
184 1986). The triple extraction procedure is optimized for samples with a BSi content < 10 µmol.
185 For some samples (cup #3, #4, #6, #7, #8, #9 and #10) the Si:Al molar ratio in the second
186 leachate was high (>10) indicating the incomplete dissolution of BSi. For these samples it was
187 not possible to use Si:Al ratios to correct for LSi leaching. A crustal Si:Al mass ratio of 3.74
188 (Taylor and McClennan, 1986) was therefore used and applied to all the samples for
189 consistency. Precision (estimated from measurement of 25 independent samples) was 13
190 nmol/mg, which represents <1 % of the BSi content in all samples and 14 % of the mean LSi

content. Blank triplicates from each extraction were below the detection limit. BSi results from this method were compared to the kinetic method from DeMaster (1981). There was an excellent agreement between the two methods (Spearman rank correlation, n = 12, p <0.001, $BSi_{kinetic} = 1.03\ BSi_{triple\ extraction} - 0.08$, data not shown). To estimate the contribution of opal to total mass flux, we assumed an opal composition of $SiO_2\ 0.4H_2O$ (Mortlock and Froelich, 1989).

In order to correct for the dissolution of BSi during deployment and storage, $Si(OH)_4$ excess was analyzed in the overlying preservative solution. Particulate BSi fluxes were corrected for dissolution assuming that excess silicic acid originated only from the dissolution of BSi phases. $Si(OH)_4$ excess was always <10 % of total (dissolved + particulate) Si concentrations. Error propagation for POC, PON, BSi fluxes and molar ratios were calculated as the quadratic sum of the relative error from triplicate measurements of each variable.

2.2 Diatom identification, fluxes and biomass

Many sediment trap studies reporting diatom fluxes in the Southern Ocean use a micropaleontological protocol that oxidizes organic material ($KMnO_4$, HCl, H_2O_2) thereby facilitating the observation of diatom valves (see Romero et al., 1999, 2000 for a description). In the present manuscript, our specific aim was to separately enumerate full and empty diatom cells captured by the sediment trap to identify key carbon or silicon exporters amongst the diatom species. We therefore used a biological method following a similar protocol to that of (Salter et al., 2007, 2012). To prepare samples for counting, 2 mL of a gently homogenized 1/8 wet aliquot were diluted in a total volume of 20 mL of artificial seawater (S = 34). In order to minimize the exclusion and/or breaking of large or elongated diatom frustules (e.g. *Thalassiothrix antarctica*), the pipette tip used for sub-sampling was modified to increase the tip aperture to >2 mm. The diluted and homogenized sample was placed in a Sedgewick-Rafter counting chamber (Pyser SGE S52, 1 mL chamber volume). Each sample was

observed under an inverted microscope (Olympus IX71) with phase contrast at 200x and 400x magnification. Diatom enumeration and identification was made from one quarter to one half of the counting chamber (depending on cell abundance). The total number of diatoms counted was >400 in all the cups with exception to the winter cup #12 (May – September 2012) where the diatom abundance was low (<100 diatoms counted). Diatoms species were identified following the recommendations of Hasle and Syvertsen (1997). All whole, intact and recognizable frustules were enumerated. Full and empty cells were counted separately, following suggestions in Assmy et al. (2013).

Due to the lower magnification used and preserved cell contents sometimes obscuring taxonomic features on the valve face, taxonomic identification to the species level was occasionally difficult and necessitated the categorizing of diatom species to genus or taxa groupings in the following manner: *Chaetoceros* species of the subgenus *Hyalochaete* resting spores (CRS) were not differentiated into species or morphotypes but were counted separately from the vegetative cells; *Fragilariopsis separanda* and *Fragilarsiopsis rhombica* were grouped as *Fragilariopsis separanda/rhombica*; *Membraneis imposter* and *Membraneis challengeri* and species of the genera *Banquisia* and *Manguinea* were denominated as *Membraneis* spp. (Armand et al., 2008a)*;* diatoms of the genus *Haslea* and *Pleurosigma* were grouped as *Pleurosigma* spp.; all *Pseudo-nitzschia* species encountered were grouped as *Pseudo-nitzschia* spp.*; Rhizosolenia antennata* and *Rhizosolenia styliformis* were grouped as *Rhizosolenia antennata/styliformis;* large and rare *Thalassiosira oliverana* and *Thalassiosira tumida* were grouped as *Thalassiosira* spp.; *Thalassiosira antarctica* resting spores (TRS) were identified separately from the vegetative cells; small centric diatoms (<20 µm) represented by *Thalassiosira gracilis* and other *Thalassiosira* species were designated as Small centrics (< 20µm); and finally large and rare centrics including *Azpeitia tabularis*, *Coscinodiscus* spp. and *Actinocyclus curvatulus* were grouped as Large centrics (>20 µm).

Full and empty frustules of each species or taxa grouping were distinguished and enumerated separately. The cell flux for each diatom species or taxa grouping was calculated according to Equation (1):

$$Cell\ flux = N_{diat} \times d\ \times 8\ \times V_{cup} \times \frac{1}{0.125} \times \frac{1}{days} \times chamber\ fraction \quad (1)$$

Where *Cell flux* is in valves m^{-2} d^{-1}, N_{diat} is the number of cells enumerated for each diatom classification, *d* is the dilution factor from the original wet aliquot, 8 is the total number of wet aliquots comprising one sample cup, V_{cup} is the volume of each wet aliquot, 0.125 is the Technicap PPS/3 sediment trap collecting area (m^2), *days* is the collecting period, *chamber fraction* is the surface fraction of the counting chamber that was observed (one quarter or one half). The annually integrated full and empty diatom flux for each species was calculated assuming as follows:

$$Annual\ flux_{(x)} = \sum_{i=1}^{12}\left(Flux_{(x)i} \times days_i\right) \quad (2)$$

Where $Annual\ flux_{(x)}$ is the annually integrated flux of a full or empty diatom species *x* (cell m^{-2} y^{-1}), $Flux_{(x)i}$ is the full or empty flux of this species in the cup number *i* (cell m^{-2} d^{-1}) and $days_i$ is the collecting time for the cup number *i* (d). The calculations assume negligible export occurred during the month of September which was not sampled by the sediment trap. We consider this assumption reasonable based on the preceding flux profile and low concentration of satellite-derived chlorophyll *a* (Rembauville et al. 2014).

We directly compared the micropaleontological (as used in Rigual-Hernández et al. (2015)) and biological counting techniques in our sediment trap samples and noted the loss of several species (*Chaetoceros decipiens, Chaetoceros dichaeta*, *Corethron pennatum Corethron inerme, Guinardia cylindrus* and *Rhizosolenia chunii)* under the

265 micropaleontological technique. We attribute this to the aggressive chemical oxidation
266 techniques used to "clean" the samples as well as the centrifugation steps which may also
267 selectively destroy or dissolve certain frustules. For the species that were commonly observed
268 by both techniques, total valve flux was in good agreement (Spearman rank correlation, n =
269 12, $\rho = 0.91$, $p < 0.001$, data not shown) although consistently lower with the
270 micropaleontolgical technique, probably due to the loss of certain frustules described above.
271 Full details of this method comparison are in preparation for a separate submission.

272 Diatoms species that contributed to more than 1 % of total full cell flux were
273 converted to carbon flux. For *E. antarctica* var. *antarctica*, *Fragilariopsis kerguelensis*,
274 *Fragilariopsis separanda/rhombica*, *Pseudo-nitzschia* spp. and *Thalassionema nitzschioides*
275 spp., we used published cell-specific carbon content ($Cell_C$, pgC cell^{-1}) for diatoms
276 communities of the Kerguelen Plateau from Cornet-Barthaux et al. (2007). As *Chaetoceros*
277 *Hyalochaete* resting spores (CRS) and *Thalassiosira antarctica* resting spores (TRS) largely
278 dominated the full diatom fluxes (>80%), an appropriate estimation of their carbon content
279 based on the specific sizes observed in our dataset was required for accurate quantification of
280 their contribution to carbon fluxes. Biomass calculations for both CRS and TRS were
281 determined from >50 randomly selected complete resting spores observed in splits from cups
282 #4 to #11 (December 2011 to May 2012). Morphometric measurements (pervalvar and apical
283 axis) were made using the Fiji image processing package (available at http://fiji.sc/Fiji) on
284 images taken with an Olympus DP71 camera. Cell volumes followed appropriate shape
285 designated calculations from Hillebrand et al. (1999) (Table 2). The cell volume coefficient of
286 variation was 46 % and 54 % for CRS and TRS, respectively. CRS carbon content was
287 estimated from the derived cell volume using the volume to carbon relationship of 0.039
288 pmolC µm^{-3} established from the resting spore of *Chaetoceros pseudocurvisetus* (Kuwata et
289 al., 1993), leading to a mean $Cell_C$ value of 227 pgC cell^{-1} (Table 2). There is currently no

290 volume to carbon relationship for *Thalassiosira antarctica* resting spores described in the
291 literature, therefore, the allometric relationship for vegetative diatoms (Menden-Deuer and
292 Lessard, 2000) was used to calculate our TRS carbon content, giving a mean $Cell_C$ value of
293 1428 pgC cell^{-1} (Table 2). Full diatom fluxes were converted to carbon fluxes as follows:

294 $$C\ flux_{(x)} = \frac{Flux_{(x)} \times Cell_{C(x)}}{M_{12_C} \times 10^9} \qquad (3)$$

295 where $C\ flux_{(x)}$ is the carbon flux carried by each diatom species *x* (mmol C m^{-2} d^{-1}), $Flux_{(x)}$ is
296 the full cell numerical flux of species *x* (cell m^{-2} d^{-1}), $Cell_{C(x)}$ is the carbon content of species *x*
297 (pgC cell^{-1}) and M_{12C} is the molecular weight of ^{12}C (12 g mol^{-1}) and 10^9 is a conversion factor
298 from pmol to mmol.

299 **2.3 Faecal pellet composition and fluxes**

300 To enumerate faecal pellets an entire 1/8 aliquot of each sample cup was placed in a gridded
301 petri dish and observed under a stereomicroscope (Zeiss Discovery V20) coupled to a camera
302 (Zeiss Axiocam ERc5s) at 10x magnification. Photographic images (2560 x 1920 pixels, 3.49
303 µm pixel^{-1}) covering the entire surface of the petri dish were acquired. Following Wilson et al.
304 (2013), faecal pellets were classified into five types according to their shape: spherical, ovoid,
305 cylindrical, ellipsoid and tabular. The flux of each faecal pellet class (nb m^{-2} d^{-1}) was
306 calculated as follows:

307 $$Faecal\ pellet\ flux = N_{FP} \times 8 \times \frac{1}{0.125} \times \frac{1}{days} \qquad (4)$$

308 where N_{FP} is the number of pellets within each class observed in the 1/8th aliquot. The other
309 constants are as described in Eq. (1). Individual measurements of the major and minor axis for
310 each faecal pellet were performed with the Fiji software. The total number of spherical, ovoid,
311 cylindrical, ellipsoid and tabular faecal pellets measured was 4041, 2047, 1338, 54 and 29,

312 respectively. Using these dimensions, faecal pellet volume was determined using the
313 appropriate shape equation (e.g. sphere, ellipse, cylinder, ovoid/ellipse) and converted to
314 carbon using a factor of 0.036 mgC mm^{-3} (Gonzalez and Smetacek, 1994). Due to the
315 irregularity of the tabular shapes preventing the use of single equation to calculate their
316 volume, a constant value of 119 µgC $pellet^{-1}$ representing a midrange value for tabular shapes
317 (Madin, 1982), was applied to tabular faecal pellets (Wilson et al., 2013). This value was
318 appropriate because the observed tabular faecal pellets were within the size range reported in
319 Madin (1982). Ranges and mean values of faecal pellet volumes and carbon content are
320 reported in Table 3. Faecal fluff and disaggregated faecal pellets were not considered in these
321 calculations because quantitative determination of their volume is difficult. We acknowledge
322 that fragmentation of larger pellets may represent an artifact of the sample splitting procedure.
323 Alternatively, their presence may also result from natural processes within the water column,
324 although dedicated sampling techniques (e.g. polyacrylamide gel traps) are required to make
325 this distinction (Ebersbach et al., 2014, 2011; Ebersbach and Trull, 2008; Laurenceau et al.,
326 2014). Consequently our present quantification of faecal pellet carbon flux should be
327 considered as lower-end estimates.

328 The precision of our calculations depends on the reliability of carbon-volume
329 conversion factors of feacal pellets, which vary widely in the literature, as well as variability
330 in diatom resting spore volumes (Table 2). To constrain the importance of this variability on
331 our quantitative estimation of C flux, we calculated upper and lower error bounds by a
332 constant scaling of the conversion factors (± 50 %).

333 **2.4 Statistical analyses**

334 Correspondence analysis was performed to summarize the seasonality of diatom export
335 assemblages. This approach projects the original variables (here full and empty cells) onto a

few principal axes that concentrate the information of the Chi-squared (Chi^2) distance between both observations and variables (Legendre and Legendre, 1998). Chi^2 distance is very sensitive to rare events. Consequently, only species with an annual mean flux higher than 10% of the mean annually integrated flux of all the species were retained in the correspondence analysis. This selection was performed separately on full and empty cell fluxes.

Partial least square regression (PLSR) analysis was used to examine the relationships between ecological flux vectors (full and empty diatom cells and faecal pellet fluxes as columns of the X matrix, cups being the rows) and bulk geochemical properties (POC flux, PON flux, BSi flux, POC:PON and BSi:POC molar ratio and columns in the Y matrix) of the exported material. The principle of PLSR is to decompose both the X and Y matrix into their principal components using principal component analysis and then use these principal components to regress Y in X (Abdi, 2010). PLSR is capable of modeling response variables from a large set of predictors. The same filter as for the correspondence analysis (full- and empty -cell fluxes >10 % of the total mean flux) was applied.

3 Results

3.1 Chemical composition of the settling material

Time series of the chemical signature of the settling material are presented in Fig. 1 and export fluxes are reported in Table 1. POC and PON fluxes are already reported and discussed in the companion paper (Rembauville et al., 2014). BSi fluxes exhibited the same seasonal pattern as POC fluxes (Fig. 1c) with low fluxes (< 1 mmol m^{-2} d^{-1}) except during the two intense events (2.60 ± 0.03 and 2.19 ± 0.10 mmol m^{-2} d^{-1}, mean ± standard deviation). LSi fluxes were highest in in spring (>10 µmol m^{-2} d^{-1} in cups #1 to #4, October to December 2011, Table 1). The contribution of LSi to total particulate Si was 5 % and 10 % respectively

in cups #1 (October/November 2011) and #12 (May to September 2012) and lower than 3 % the remainder of the year. The BSi:POC molar ratio was highest at the beginning of the season (between 2.18 ± 0.19 and 3.46 ± 0.16 in the first three cups from October to December 2011, blue line in Fig. 1c) and dropped to 0.64 ± 0.06 in cup #5 (end December 2011), following the first export event. BSi:POC ratios were close in the two export events (1.62 ± 0.05 and 1.49 ± 0.08). The lowest BSi:POC ratio was observed in autumn in cup #11 (0.29 ± 0.01, February to May 2012). Similarly, the opal contribution to total mass flux was highest in spring (70.8 % in cup #2, November 2011) and lowest in autumn (21.5 % in cup #11, February to May 2012).

3.2 Diatom fluxes

Diatoms from 33 taxa were identified and their fluxes determined across the 11-months time series. Fluxes are reported in Table 4 and Table 5 for full and empty cells, respectively. Full and empty cell fluxes for the total community and for the taxa that are the major contributors to total diatom flux (eight taxa that account for >1 % of total cells annual export) are presented in Fig. 2. The full and empty cell fluxes for each diatom species or taxa are reported in Table 4 and 5, respectively.

During spring (cups #1 to #3, October to December 2011) and autumn/winter (cups #11 and #12, February to September 2012) the total flux of full cells was $< 5 \times 10^6$ cells m^{-2} d^{-1} (Fig. 2a). The total flux of full cells increased to 5.5 and 9.5×10^7 cells m^{-2} d^{-1} (cups #4 and #9, December and end January respectively) during two episodic (<14 days) sedimentation events. The two largest flux events (cups #4 and #9) were also associated with significant export of empty cells with respectively 6.1×10^7 and 2.9×10^7 cells m^{-2} d^{-1} (Fig. 2a). For *Chaetoceros Hyalochaete* spp. resting spores (CRS), full cells fluxes of 4×10^7 cells m^{-2} d^{-1} and 7.8×10^7 cells m^{-2} d^{-1} accounted for 76 % and 83 % of the total full cell flux during these

two events, respectively (Fig. 2b), whereas a smaller contribution of *Thalassiosira antarctica* resting spores (TRS) (2.7×10^6 cells m^{-2} d^{-1}, 5 % of total full cells) was observed during the first event (Fig. 2h). CRS also dominated (79-94 %) the composition of full cells in the intervening period (cups #5-#8, December 2011 to January 2012), although the magnitude of cell flux was moderate ($9 \times 10^6 – 2.5 \times 10^7$ cells m^{-2} d^{-1}) by comparison (Fig. 2b). In cup #4 (December 2011), the empty cell flux contained 61 % of *C. Hyalochaete* spp. vegetative empty cells and 27 % of unidentified Small centrics (<20 µm) empty cells. In cup #9 (end January 2012), the total empty cells flux contained 60 % of *C. Hyalochaete* spp. vegetative stage and only 2 % of Small centrics (<20 µm) empty cells.

Fragilariopsis kerguelensis, and *Fragilariopsis separanda/rhombica* (Fig. 2d and 2e) were mostly exported from spring through the end of summer (cups #1 to #10, October 2011 to February 2012) with total (full + empty) fluxes < 3×10^6 cells m^{-2} d^{-1}, a value ~20 times lower than the highest CRS fluxes recorded. During this time, these species were represented by >50 % of empty cells. In autumn and winter, (cups #10 and #11, February to May 2012), these species were only represented by low fluxes (< 0.5×10^{-6} cells m^{-2} d^{-1}) of empty cells. *Thalassionema nitzschioides* spp. fluxes were highest in spring and early summer (cups #1 to #4, October to December 2011) with total fluxes comprised between 3.5×10^6 and 6.7×10^6 cells m^{-2} d^{-1} (Fig. 2g). The remainder of the year, total flux was < 2×10^6 cells m^{-2} d^{-1} and was essentially represented by full cells. *Pseudo-nitzschia* spp. were mostly represented by full cells (Fig. 2f) with the highest flux of 1.2×10^7 cells m^{-2} d^{-1} observed in the second intense export event (cup #9, end January 2012). *Eucampia antarctica* var. *antarctica* total fluxes were always represented by >50 % of full cells (Fig. 2c). Total cell fluxes of *Eucampia antarctica* var. *antarctica* gradually increased from <1×10^5 to 1.3×10^6 cells m^{-2} d^{-1} from spring to summer (cups #1 to #9, October 2011 to January 2012) and then decreased to a negligible flux in winter (cup #12, May to September 2012). This species was observed as

409 both the lightly silicified, chain-forming, vegetative form and the highly silicified winter
410 growth stage form. Both forms were observed throughout the year without specific seasonal
411 pattern. Small centric species (<20 µm) were essentially represented by empty cells (Fig. 2i).
412 Their total fluxes were $<4 \times 10^6$ cells m^{-2} d^{-1}, except in the first export event (cup #4,
413 December 2011) where their flux represented a considerable export of 1.7×10^7 cells m^{-2} d^{-1}.

414 Diatoms and sampling cup projection on the first two axes from the correspondence
415 analysis is presented in Fig. 3. Chi² distance in the correspondence analysis is based on
416 frequency distribution, therefore the results of the analysis must be considered as
417 representative of the community composition as opposed to cell flux. The first two factors
418 accounted for the majority (75.6 %) of total explained variance. Early in the season (cups #1-
419 #3, October to mid-December 2011), during the period of biomass accumulation in the
420 surface (Fig 1a), diatom fluxes were characterized by empty cells of *T. nitzschioides* spp. and
421 *F. kerguelensis.* Full TRS cells were observed in cup #3 (end November 2011) following the
422 initial bloom decline. The first major flux event (cup #4, December 2011) contained mostly
423 TRS, empty Small centrics (< 20 µm) cells and empty *C. Hyalochaete* spp. cells. The summer
424 flux period (cups #5 to #8, December 2011 to January 2012) primarily consisted of CRS,
425 although *E. antarctica* var. *antarctica, Pseudo-nitzschia* spp, and *Thalassiothrix antarctica*
426 were present as full cells and *Plagiotropis* spp., *Membraneis* spp., *Pseudo-nitzschia* spp. as
427 empty cells. The second major flux event (cup #9, end January 2012) was tightly associated
428 with CRS and full *Pseudo-nitzschia* spp. cells. Subsequent cups (#10 and #11, February to
429 May 2012) were characterized by full cells of *E. antarctica* var. *antarctica* and *Thalassiotrix*
430 *antarctica* and empty cells of *Corethron inerme*, *P. alata*, *F. separanda/rhombica* and *F.*
431 *kerguelensis*. Winter fluxes (cup #12, May to September 2012) were similar to the initial three
432 cups characterized primarily by empty cells of small diatom taxa. The centralized projection

433 in Fig. 3 of full *F. kerguelensis* and *T. nitzschioides* spp. highlights their constant presence
434 throughout the annual record.

435 The total empty:full cell ratio is presented in Fig. 2a (blue line). This ratio was highest
436 in spring and early summer (cups #1 to #4, October to December 2011), ranging between 1.1
437 and 2.4, suggesting more empty cells to full cells. The ratio was lowest, representing
438 considerably more full cells to empty cells in cups #5 to #10 (December 2011 to February
439 2012) with values between 0.1 and 0.4. In autumn (cup #11, February to May 2012), the
440 empty:full ratio increased to 0.7. In the winter cup #12 (May to September 2012), the total
441 amount of full diatom cells was very low and therefore we could not calculate a robust
442 empty:full ratio. Across the time-series certain diatom taxa were observed exclusively as
443 empty cells, notably *Chaetoceros atlanticus* f. *bulbosum*, and *Corethron pennatum*. For
444 diatom taxa present as full and empty cells we calculated an annually integrated empty:full
445 ratio (Fig. 4) and arbitrarily defined threshold values of 2 (representing species mainly
446 observed as empty cells) and 0.5 (representing species mainly observed as full cells),
447 respectively. In decreasing order, the diatom taxa exhibiting empty:full ratios >2 were
448 *Thalassiosira lentiginosa*, Small centrics (<20 µm), *Proboscia alata*, *Rhizosolenia*
449 *antennata/styliformis*, *Chaetoceros decipiens*, *Corethron inerme*, *Dactyliosolen antarcticus*,
450 Large centrics (>20 µm), and *Asteromphalus* spp. The diatom taxa displaying an empty:full
451 ratio <0.5 were *Thalassiothrix antarctica*, *Rhizosolenia simplex*, CRS, *Eucampia antarctica*
452 var. *antarctica*, *Thalassiosira* spp. and *Navicula* spp. Species or grouped taxa with ratio
453 values falling between the thresholds <2 and >0.5 (*R. chunii*, through to *C. dichaeta* in Fig. 4)
454 were perceived as being almost equally represented by full and empty cells when integrated
455 annually across the time series.

456 **3.3 Faecal pellet fluxes**

457 The seasonal flux of faecal pellet type, volume and their estimated carbon flux are
458 summarized in Fig. 5 and Table 6. Total faecal pellet flux was $<2 \times 10^3$ pellets m^{-2} d^{-1} in
459 spring (cups #1 to #3, October to December 2011). Cups #4 and #5 (December 2011) were
460 characterized by the highest fluxes of 21.8×10^3 and 5.1×10^3 pellets m^{-2} d^{-1} (Fig. 5a, Table
461 6). Faecal pellet numerical flux decreased gradually from mid-summer (cup #5, December
462 2011) to reach a minimal value in winter (140 pellets m^{-2} d^{-1} in cup #12, May to September
463 2012). In spring (cups #1 to #3, October to December 2011), spherical and cylindrical shapes
464 dominated the numerical faecal pellet fluxes. Ellipsoid and tabular shapes were absent from
465 these spring cups. The first export event (cup #4, December 2011), was numerically
466 dominated by the spherical shaped pellets, however the remainder of the summer (cups #5 to
467 #10, December 2011 to February 2012) contained spherical, ovoid and cylindrical shapes in
468 comparable proportions. Ellipsoid shapes were observed from mid-summer to autumn (cups
469 #7 to #11, January to May 2012) but their overall contribution to pellet flux was low (<6 %,
470 Table 6). Rare tabular shapes were observed in summer (cups #6 and #8, December and
471 January 2012) and their contribution to numerical fluxes was highest in autumn and winter
472 (cups #11 and #12, February to September 2012).

473 The median faecal pellet volume showed a seasonal signal with a maximum peak >5.5
474 $\times 10^6$ μm^3 in mid-summer (cups # 6 to #8, mid-December to January 2012) and values $<4 \times$
475 10^6 μm^3 the remainder of the year (Fig. 5b). Concomitantly with the highest median volume,
476 the largest variance in faecal pellet size was also observed in the summer (highest
477 interquartile values in Fig. 5b).

478 Total faecal pellet carbon flux was lowest in spring (<0.05 mmolC m^{-2} d^{-1} in cups #1
479 to #3, October to December 2011, Fig. 5c, Table 6). The highest total faecal pellet carbon flux
480 of nearly 0.5 mmolC m^{-2} d^{-1} was observed during the first export event in cup #4 (December
481 2011) and was essentially composed of spherical shapes (83 %, Table 6). For the remainder of

the summer (cups #5 to #10, December 2011 to February 2012), total faecal pellet carbon flux was between 0.03 and 0.15 mmolC m^{-2} d^{-1} with a dominant contribution of cylindrical, ellipsoid and tabular shapes. In autumn and winter (cups #11 and #12, February to September 2012), faecal pellet carbon fluxes of 0.13 and 0.06 mmolC m^{-2} d^{-1} were strictly dominated by tabular shapes (>90 % to total faecal pellet carbon fluxes, Table 6).

3.4 Statistical analysis of biological and biogeochemical signatures

The β correlation coefficients of standardized variables obtained from the PLSR analysis are presented as a heatmap in Fig. 6. The full cell fluxes of all diatom taxa, in addition to spherical and ovoid and ellipsoid faecal pellet fluxes were positively correlated to POC and PON fluxes. By contrast, empty cell fluxes of *F. kerguelensis*, *P. alata*, *T. nitzschioides* spp., *T. lentiginosa* and cyclindrical, ellipsoid and tabular pellet fluxes were either uncorrelated or negatively correlated with POC and PON fluxes. Full- and empty-cell fluxes of all diatom taxa were positively correlated with BSi fluxes, although this correlation was notably weak for empty cells of *C. inerme*, *P. alata* and *T. lentiginosa*. Only spherical and ovoid faecal pellets were positively correlated with BSi fluxes. Full cells fluxes of CRS and *E. antarctica* var. *antarctica* were the most negatively correlated with BSi:POC molar ratio, whereas TRS, *F. kerguelensis*, *T. nitzschioides* spp. and *T. lentiginosa* full cells fluxes were positively correlated. Spherical and ovoid faecal pellets were weakly and negatively correlated with the BSi:POC molar ratio whereas the cylindrical, ellipsoid and tabular shapes were more strongly negatively correlated to the BSi:POC molar ratio. All the biological components exhibited weak or no correlations to the POC:PON molar ratio.

The first two latent vectors of the PLSR accounted for 61.3 % and 74.1 % of cumulative variance in X (full and empty diatom and pellet fluxes) and Y (biogeochemical properties). In order to visualize how the seasonal succession of flux vectors was related to

506 the bulk geochemical properties of particles, the sampling cups, biological and chemical
507 factors were projected on the first two latent factors of the PLSR analysis (Fig. 7). Positively
508 projected on the first axis are the POC, PON and BSi fluxes, close to the export events
509 sampled in cups #4 (December 2011) and #9 (end January 2012). The closest biological
510 components comprise a complex assemblage of full and empty cells and spherical and ovoid
511 faecal pellet shapes. All the other cups are projected far from these two export events. The
512 second axis opposes the spring cups (#1 to #3, October to mid-December 2011) to the autumn
513 (#11, February to May 2012) and winter (#12, May to September 2012) cups. Empty frustules
514 of *F. kerguelensis*, *T. lentiginosa* and *T. nitzschioides* spp. are projected close to the spring
515 cups (#1 to #3, October to mid-December 2011) together with the BSi:POC molar ratio
516 whereas autumn (#11, February to May 2012) and winter cups (#12, May to September 2012)
517 are projected far from the BSi:POC molar ratio and close to the tabular and cylindrical faecal
518 pellet shapes.

519 **3.5 Partitioning carbon fluxes among ecological vectors**

520 We estimated the contribution of resting spores and faecal pellets to carbon flux, calculated
521 their cumulative values and compared them to measured values (Fig. 8a and 8b). A highly
522 significant correlation (Spearman rank correlation, n= 36, $\rho = 0.84$, $p < 0.001$) was evident
523 between calculated and measured carbon flux suggesting that the main ecological flux vectors
524 observed in the sample were capable of explaining the seasonal variation in total POC flux.
525 Table 7 lists the contribution of each vector to the calculated flux. In cup #1 (October to mid-
526 November 2011), CRS and other diatoms dominated the calculated POC fluxes, with
527 respectively 25.3 % and 38.6 %. Diatoms other than spores dominated the calculated carbon
528 flux (35.4 %) together with cylindrical faecal pellets (36.4 %) in cup #2 (November 2011).
529 TRS dominated the POC fluxes (85.1 %) in cup #3 (November/December 2011). CRS strictly
530 dominated the calculated POC fluxes in summer (cups #4 to #10, December 2011 to February

2012) with a contribution ranging from 46.8 % to 88.1 %. During the autumn and winter (cups #11 and #12, February to September 2012), POC fluxes were almost exclusively associated to tabular faecal pellets, 81 % and 93.3 %, respectively. At annual scale diatoms resting spores (CRS and TRS), other diatoms and faecal pellets respectively accounted for 60.7 %, 5 % and 34.3 % of the calculated POC fluxes. Annual POC fluxes estimated from ecological vectors considered here were slightly less than measured values (93.1 versus 98.2 mmol m^{-2}).

4 Discussion

4.1 The significance of resting spores for POC flux

In a companion paper we present multiple lines of evidence that converge on a scenario of strong flux attenuation between the base of the winter mixed layer (WML at ~220 m) and 300 m on the Kerguelen Plateau (Rembauville et al., 2014). Most notably large attenuation coefficients (3.3 – 4) were calculated from independent measurements in spring and summer (Ebersbach and Trull, 2008; Jouandet et al., 2014). Strong flux attenuation and under trapping due to hydrodynamics and swimmers combine to explain the low annually-integrated POC fluxes. Generally POC fluxes were <0.5 mmol m^{-2} d^{-1} with the notable exception of two pulsed (<14 days) export events of ~1.5 mmol m^{-2} d^{-1} that accounted for ~40 % of annual POC export. These two flux events were characterized by a noticeable increase and general dominance of diatom resting spores. During both of these pulsed export events, cumulative *Chaetoceros Hyalochaete* spp. resting spores (CRS) and *Thalassiosira antarctica* resting spores (TRS) fluxes accounted for 66 % and 88 % of the measured POC flux, whereas total faecal pellet flux accounted for 29 % and 5.2 %, respectively (Table 7). The combination of CRS and TRS were responsible for 60.7 % of the annual calculated POC flux, a value ten times higher than the contribution of other diatoms (5 %). We did not observe any full cells of

555 the vegetative stage of *Chaetoceros Hyalochaete*, a feature possibly related to its high
556 susceptibility to grazing pressure in the mixed layer (Smetacek et al., 2004; Quéguiner, 2013;
557 Assmy et al., 2013). Empty *Chaetoceros Hyalochaete* spp. cells were vegetative stages
558 different in shape from the resting spores. These empty frustules may be the remnants of
559 vegetative stages following spore formation. Alternatively, dissolution of the lightly silicified
560 valves or girdle bands of the vegetative cell could result in the rapid consumption of the
561 cellular organic material in the upper water column and this may also explain the absence of
562 full vegetative cells in the sediment trap record. Our flux data reveal that small (10 to 30 µm)
563 and highly silicified resting spores bypass the intense grazing pressure characterizing the base
564 of the mixed layer, and are the primary mechanism through which carbon and, to a lesser
565 extent silicon, is exported from the surface.

566 Numerous sediment trap studies have reported a strong contribution, if not dominance,
567 of CRS to diatom fluxes at depth in various oceanographic regions: firstly, in coastal
568 influenced regions (e.g. Antarctic Peninsula (Leventer, 1991), Bransfield Strait (Abelmann
569 and Gersonde, 1991), Gulf of California (Sancetta, 1995), the Omura Bay (Kato et al., 2003),
570 North Pacific Ocean (Chang et al., 2013) and the Artic (Onodera et al., 2014)), secondly in
571 upwelling-influenced regions (e.g. Santa Barbara basin (Lange, 1997), Eastern Equatorial
572 Atlantic (Treppke et al., 1996)) and finally in the open ocean in the subarctic Atlantic
573 (Rynearson et al., 2013). Similar to sediment trap observations, CRS are reported as dominant
574 in surface sediments of coastal regions (peri-Antarctic shelf and Antarctic sea ice (Crosta et
575 al., 1997; Zielinski and Gersonde, 1997; Armand et al., 2005), the North Scotia Sea (Allen et
576 al., 2005) and east of Kerguelen Island (Armand et al., 2008b)), but also in upwelling-
577 influenced regions (the northeastern Pacific (Grimm et al., 1996), the northeast Pacific (Lopes
578 et al., 2006)) and finally in the open ocean (the North Atlantic, Bao et al., 2000). Moreover,
579 the annual POC export from the A3 station sediment trap at 289 m (98.2±4.4 mmol m^{-2} y^{-1})

falls near annual estimates from deep sediment traps (>2000 m) located in the naturally fertilized area downstream of the Crozet Islands (37-60 and 40-42 mmol m^{-2} y^{-1}, Salter et al., 2012) where fluxes were considered as mainly driven by resting spores of *Eucampia antarctica* var. *antarctica*. Diatom resting spores are frequently observed in blooms heavily influenced by the proximity of the coast. Major resting spores contribution to carbon fluxes was observed in only one study in the open North Atlantic Ocean (Rynearson et al., 2013), but they are generally absent or very rare in open ocean sediment trap studies (Fischer et al., 2002; Grigorov et al., 2014; Rigual-Hernández et al., 2015). The frequent occurrence and widespread distribution of diatoms resting spores in the neritic or coastal-influenced ocean suggest their pivotal role in the efficient transfer of carbon to depth in these areas.

Chaetoceros resting spores have been reported to contain up to 10 times more carbon than the vegetative forms (Kuwata et al., 1993) with no vacuole and high contents of lipids and carbohydrates (Doucette and Fryxell, 1983; Kuwata et al., 1993). Moreover, CRS resist grazing and have been found to lower copepods grazing pressure (Kuwata and Tsuda, 2005). We suggest that diatom resting spores gather three essential characteristics for effective POC export to the deep ocean: (1) they efficiently bypass the grazing pressure near the mixed layer due to their morphological characteristics such as very robust frustules (CRS) or numerous spines (TRS) (high export efficiency), (2) they are efficiently transferred to depth due to the thick and dense frustule increasing sinking velocity and (3) their high carbon content is protected from microbial degradation by the thick frustules (these last two points result in a high transfer efficiency). The spatial distribution and formation of resting spores may therefore be an integral ecological component defining the strength and efficiency of the biological pump in specific regions. Nutrient depletion has been shown to trigger resting spore formation in *Chaetoceros Hyalochaete* laboratory cultures (Garrison, 1981; Sanders and Cibik, 1985; Kuwata et al., 1993; Oku and Kamatani, 1997) over relatively rapid timescales

(6 to 48 h, McQuoid and Hobson, 1996). Although $Si(OH)_4$ depletion appears to be the most likely biogeochemical trigger at the Kerguelen Plateau (from 24 µmol L^{-1} in early spring to 2 µmol L^{-1} in summer, (Mosseri et al., 2008; Closset et al., 2014)), other environmental factors (iron or light availability) could influence the resting spore formation. Notably, dissolved iron concentration in the mixed layer rapidly decreases to 0.1~0.2 nmol L^{-1} after the beginning of the spring bloom at A3, however the vertical entrainment is much weaker in summer compared to spring (Bowie et al., 2014). Further work to establish seasonal dynamics of these factors linked to diatom life cycles and specifically the formation of resting spore is necessary.

4.2 Contribution of faecal pellets to POC flux

Although diatom resting spores are the primary vector for POC flux below the mixed layer, faecal pellets were also important and accounted for 34.3 % of annual export. It has been hypothesized that faecal pellets are the dominant flux component in High Biomass, Low Export (HBLE) environments, where biomass is routed to higher trophic levels (Lam and Bishop, 2007; Ebersbach et al., 2011). However, this hypothesis does not appear to be true for the bloom of the central Kerguelen Plateau suggesting that faecal material is efficiently reprocessed in the mixed layer, or that a significant part of the pellet flux is excreted below the trap depth by vertically migrating zooplankton. Small spherical faecal pellets dominated the annual numerical faecal pellet flux (53.8 %, Table 6). The short and intense export of small spherical faecal pellets was concomitant with the first strong POC export in cup #4 (December 2011, Table 6). The significance of small spherical faecal pellets to POC flux is somewhat uncharacteristic in comparison to other sediment trap records in shallow areas of the Southern Ocean (Schnack-Schiel and Isla, 2005). They are possibly produced by small cyclopoid copepods, like *Oithona similis* that are abundant in the POOZ (Fransz and Gonzalez, 1995; Pinkerton et al., 2010). More specifically, *O. similis* represents >50 % of

mesozooplankton abundance at A3 in spring (Carlotti et al., 2015) has been observed at station A3 in summer (Carlotti et al., 2008). *Oithona* species are known to be coprophagous and play an important role in flux reprocessing (Gonzalez and Smetacek, 1994), which may partially contribute to the rapid flux attenuation observed by efficiently retaining carbon in the mixed layer. This reprocessing feeding strategy might also explain the low faecal pellet flux we observed (highest value of 21.8×10^3 pellet m^{-2} d^{-1}), which was two orders of magnitude lower than the $>5 \times 10^5$ pellet m^{-2} d^{-1} observed in neritic areas where euphausiids dominate the mesozooplankton community (Bodungen, 1986; von Bodungen et al., 1987; Wefer et al., 1988).

There were notable differences in faecal pellet type over the course of the season. The transition from spherical and ovoid pellets in spring to larger cylindrical and tabular pellets in summer presumably reflects shifts in dominant zooplankton species from small cyclopoid copepods towards larger calanoid copepods, euphausiids and salps (e.g. Wilson et al., 2013). Carlotti et al. (2015) report that mesozooplankton biomass doubled between October and November 2011 and was three-fold higher in January 2005 (Carlotti et al., 2008). In spring, Carlotti et al. (2015) observed that the small size fraction (300 – 500 µm) was numerically dominated by *Oithona similis* (50 % of the total mesozooplankton assemblage), although the larger size fractions dominated the mesozooplankton biomass (dominated by *Clausocalanus citer*, and *Rhicalanus gigas*). This is consistent with the dominance of small spherical faecal pellets and the lower contribution of cylindrical shapes we observed in spring and early summer (cups #1 to #4, October to December 2011, Table 6). In summer (January 2005), the mesozooplankton community was more diversified and comprised 21 % of small individuals (*Oithona* sp and *Oncea* sp.), 20 % of medium-sized individuals (*Clausocalanus* sp and *Microcalanus* sp.) and 21 % of large individuals (*Calanus* sp., *Metrida* sp., *Paraeuchaeta* sp., *Pleuromama* sp. and *Rhincalanus* sp.; Carlotti et al., 2008). As the median size of faecal

pellets increases, so does their relative contribution to carbon flux (Fig. 5b and 5d, Table 6). Our observation of an increasing contribution of cylindrical faecal pellet shapes in summer (cups #5 to #10, December 2011 to February 2012, Table 6) is consistent with the increasing contribution of large calanoid copepods to the mesozooplankton assemblages. We note that pteropods showed the highest contribution to mesozooplankton assemblages at station A3 in summer (16 % of total abundance, Carlotti et al., 2008). We associate this observation with the large ellipsoid faecal pellet shape that was first observed in the sediment trap in cup #5 (end December 2011) and represented the highest contribution to faecal pellet carbon fluxes in cup #9 (January/February 2012, Table 7). Tabular faecal pellets dominated the low POC fluxes observed in the autumn and winter when chlorophyll *a* concentration was reduced to background levels, although this interpretation should be taken with caution since a constant and high carbon content was used for this shape. The increase in organic carbon content and negative correlation between the abundance of cylindrical, ellipsoid and tabular faecal pellets fluxes and the BSi:POC molar ratio suggests that large zooplankton producing these tabular pellets (large copepods, euphausiids and salps) were not feeding directly on diatoms. During the autumn and winter, microbial components other than diatoms must sustain the production of these large zooplankton. Direct observation of faecal pellet content is beyond the scope of the present study but would help to elucidate how seasonal trends of zooplankton feeding ecology influence carbon and biomineral export. Moreover, dedicated studies are still needed to document the seasonal dynamic of euphausiid and salp abundances over the Kerguelen Plateau to compare them with our reported faecal pellet fluxes.

4.3 Diatom fluxes

The diatom fluxes (sum of empty and full cells) observed at the central Kerguelen Plateau reached their maximum value of 1.2×10^8 cells m^{-2} d^{-1} during the two short export events, which is equivalent to 2.4×10^8 valves m^{-2} d^{-1}. This latter value falls between the

680 highest values observed in POOZ (~10^7 valves m^{-2} d^{-1} Abelmann and Gersonde, 1991; Salter
681 et al., 2012; Grigorov et al., 2014) and the SIZ (>10^9 valves m^{-2} d^{-1}, Suzuki et al., 2001;
682 Pilskaln et al., 2004). The diatom fluxes over the Kerguelen plateau are similar to the 2.5 - 3.5
683 × 10^8 valves m^{-2} d^{-1} measured at 200 m depth in a coastal station of the Antarctic Peninsula,
684 where CRS represented ~80 % of the phytoplankton assemblage (Leventer, 1991). Previous
685 studies report the presence of a resting spore formation strategy in diatom species as typically
686 associated with neritic areas (Smetacek, 1985; Crosta et al., 1997; Salter et al., 2012). During
687 the summer KEOPS1 cruise, a shift in plankton community composition was observed at
688 station A3 between January and February. The surface community initially dominated by
689 *Chaetoceros Hyalochaete* vegetative chains gave way to one dominated by *Eucampia*
690 *antarctica* var. *antarctica*, concomitant with increasing CRS abundance in the mixed layer
691 (Armand et al., 2008a). The abundance of dead cells (within chains or as empty single cells
692 and half cells) in the surface water column also increased from January to February,
693 suggesting intense heterotrophic activity. Surface sediments at station A3 contain, in
694 decreasing abundance, *F. kerguelensis*, CRS and *T. nitzschioides* spp. cells (Armand et al.,
695 2008b). These sedimentary distributions are consistent with the dominant species observed in
696 the sediment trap, *F. kerguelensis* and *T. nitzschioides* spp. being present throughout the year
697 and mostly represented by empty cells whereas CRS are exported during short and intense
698 events.

699 *Eucampia antarctica* var. *antarctica* resting spores dominated the deep (2000 m)
700 sediment trap diatom assemblages in the naturally fertilized area close to the Crozet Islands
701 with fluxes > 10^7 cells m^{-2} d^{-1} (Salter et al., 2012). We observed highest *Eucampia antarctica*
702 var. *antarctica* full cells fluxes of ~10^6 cells m^{-2} d^{-1} in summer, which represents <10 % of the
703 total cell flux. Both vegetative and resting stages were observed. Our results suggest that
704 *Eucampia antarctica* var. *antarctica* is unlikely to be a major driving vector for carbon fluxes

to depth over the central Kerguelen Plateau, in part because the community was not forming massive highly-silicified, fast-sinking resting spores contrary to observations near the Crozet Islands. Moreover their biogeographic abundance distribution from sea floor observations suggests they are not dominant in this region of the plateau (Armand et al., 2008b). The iron-fertilized Crozet bloom is north of the Polar Front and dissolved $Si(OH)_4$ concentrations were depleted to 0.2 μmol L^{-1} (Salter et al., 2007) compared to ~2 μmol L^{-1} on the Kerguelen Plateau (Mosseri et al., 2008). It is possible, along with differences in iron dynamics between the two plateaus, that differences in nutrient stoichiometry favour bloom dynamics and resting spore formation of *Chaetoceros Hyalochaete* populations surrounding the Kerguelen Islands. Nevertheless, the increasing full cell flux of *Eucampia antarctica* var. *antarctica* from spring to summer in the sediment trap time series is consistent with the observations of an increasing abundance in the mixed layer at the station A3 in summer (Armand et al., 2008a).

Highest *Pseudo-nitzschia* spp. full cell fluxes were observed in summer, concomitantly with the second export peak (cup #9, end January 2012). *Pseudo-nitzschia* species are rarely found in deep sediment trap studies and are absent from sediment diatom assemblages, presumably due to their susceptibility to water column dissolution (Grigorov et al., 2014; Rigual-Hernández et al., 2015). The species *Pseudo-nitzschia hemii* has been reported to accumulate in summer in deep chlorophyll maximum in the Polar Frontal Zone (Kopczynska et al., 2001). Such deep biomass accumulation is hypothesized to benefit from nutrient diffusion through the pycnocline (Parslow et al., 2001). These general observations are consistent with the peaks in *Pseudo-nitzschia* spp. fluxes we report in summer over the Kerguelen Plateau.

Although their fluxes were very low, species of the *Rhizosolenia* and *Proboscia* genera were mostly exported as empty cells at the end of summer and during autumn (cups #8 to #11, end January to May 2012), occurring in parallel with the full cell fluxes of the giant

730 diatom *Thalassiothrix antarctica* (Table 4). It has been suggested that these species belong to
731 a group of "deep shade flora" that accumulate at the subsurface chlorophyll maxima in
732 summer with their large frustules protecting them from grazing pressure in stratified waters
733 (Kemp and Villareal, 2013). Interestingly these species were also found in deep sediment
734 traps located in a HNLC area south of the Crozet Plateau (Salter et al., 2012), as well as in
735 subsurface chlorophyll maximum in HNLC waters of the Southern Ocean (Parslow et al.,
736 2001; Holm-Hansen et al., 2004; Gomi et al., 2010). A subsurface chlorophyll maximum has
737 previously been observed at 120 m on the Kerguelen Plateau (also station A3) during summer
738 (Uitz et al., 2009) and appears to correspond to an accumulation of particles consisting of
739 aggregates of large diatom species (Jouandet et al., 2011). The fact that *Rhizosolenia* spp. and
740 *Proboscia* spp. were observed as empty cells whereas *Thalassiothrix antarctica* was mostly
741 represented by full cells suggest species-specific grazing on these communities. There appears
742 to be ecological differentiation within the "deep shade flora" that precludes describing a
743 single effect on export stoichiometry. Moreover, on the Kerguelen Plateau, these species are
744 not exported in "massive" proportions as the fall-dump hypothesis suggests (Kemp et al.,
745 2000). The physical and biogeochemical factors responsible for their production and export
746 are still to be determined, and should be investigated thoroughly given the potential
747 importance that these species might have for export fluxes on a global scale (Kemp et al.,
748 2000; Richardson et al., 2000; Kemp and Villareal, 2013).

749 **4.4 Preferential carbon and silica sinkers**

750 Unlike most previous sediment trap studies in the Southern Ocean, we used a counting
751 technique that facilitated the identification of carbon and siliceous components of exported
752 material. Although we lost a small degree of taxonomic resolution with this approach (see
753 methods), it allowed us to avoid unnecessary assumptions concerning carbon content of

754 exported diatoms and directly constrain the role of different species for carbon and silica
755 export.

756 The annual BSi:POC ratio of the exported material (1.16) is much higher than the
757 usual ratio proposed for marine diatoms of 0.13 (Brzezinski, 1985). Moreover, the BSi:POC
758 ratio of the exported material in spring (2.1 to 3.4, cups #1 to #3, October to mid-December
759 2011) is significantly higher than the BSi:POC ratio of 0.32 ± 0.06 in the mixed layer of the
760 same station during spring (Lasbleiz et al., 2014). Numerous chemical, physical, biological
761 and ecological factors can impact BSi:POC ratios of marine diatoms (e.g. Ragueneau et al.,
762 2006). However, the ten-fold differences in BSi:POC ratios of exported particles between
763 spring and summer is unlikely to result only from physiological constraints set during diatoms
764 growth (Hutchins and Bruland, 1998; Takeda, 1998). Previous comparisons in natural and
765 artificially iron-fertilized settings have the highlighted importance of diatom community
766 structure for carbon and silica export (Smetacek et al., 2004; Salter et al., 2012; Quéguiner,
767 2013; Assmy et al., 2013). The presence of different diatom species and their characteristic
768 traits (e. g. susceptibility to grazing, apoptosis, viral lysis) are all likely to influence the flux
769 of full and empty cells. Therefore, the net BSi:POC export ratio results from the net effect of
770 species specific Si:C composition (Sackett et al., 2014) and the subsequent species-specific
771 mortality pathway and dissolution. A significant correlation between BSi:POC and empty:full
772 cells ratio (Spearman rank correlation, $n = 12$, $\rho = 0.78$, $p < 0.05$) suggests the latter acts as a
773 first order control on the silicon and organic carbon export stoichiometry. Differences in
774 BSi:POC ratios between the mixed layer suspended particle stock and particles exported out
775 the mixed layer may be explained by the dominant sedimentation of empty diatom frustules
776 that results from the grazing pressure by the zooplankton community and the intense carbon
777 utilization by heterotrophic microbial communities (Christaki et al., 2014).

We classified species that were observed exclusively as empty cells, or sinking with an integrated empty:full ratio >2, as predominantly silica exporters and these included: *C. bulbosum, C. pennatum, P. truncata, R. antennata/styliformis, A. hookeri, A. hyalinus, C. decipiens, C. inerme, D. antarcticus, P. alata, T. nitzschioides* spp., *T. lentiginosa*, and small centric species (< 20 µm). Although *F. kerguelensis, T. nitzschoides spp.* and *T. lentiginosa* were present through the entire season, their fluxes were highly correlated with BSi:POC ratios (Fig. 6) identifying these species as significant contributors to silica export. On the contrary resting spores and species that sink with a major contribution of full cells (integrated empty:full ratio <0.5) were identified as belonging to the preferential carbon sinkers: *C. Hyalochaete* spp., *E. antarctica* var. *antarctica*, *R. simplex* and *Thalassiothrix antarctica*. Among them, CRS and *E. antarctica* var. *antarctica* were the most negatively correlated to the BSi:POC ratio and were identified as key species for carbon export (Fig. 6). These observations are consistent with a previous study of natural iron fertilization that identified *C. pennatum, D. antarcticus* and *F. kerguelensis* as major silica sinkers and CRS and *E. antarctica* var. *antarctica* resting spores as major carbon sinkers downstream Crozet islands (Salter et al., 2012). During the EIFEX artificial fertilization experiment *C. Hyalochaete* vegetative stages were identified as major carbon sinker whereas *F. kerguelensis* was considered as strong silica sinker (Assmy et al., 2013). Notably, resting spore formation was not observed in the artificial experiment performed in the open ocean remote from coastal influence, and carbon export was attributed to mass mortality and aggregation of algal cells (Assmy et al., 2013). Nevertheless, a more detailed analysis of species-specific carbon and silica content in the exported material is necessary to fully elucidate their respective roles on carbon and silica export.

4.5 Seasonal succession of ecological flux vectors over the Kerguelen Plateau

802 Although sediment trap records integrate cumulative processes of production in the mixed
803 layer and selective losses during export, they provide a unique insight into the temporal
804 succession of plankton functional types and resultant geochemical properties of exported
805 particles characterizing the biological pump. The seasonal cycle of ecological vectors and
806 associated export stoichiometry is summarized in Figure 7. The robustness of the relationship
807 between measured and calculated POC fluxes (Fig. 8b) suggests that the main ecological flux
808 vectors described from the samples are capable of predicting seasonal patterns of total POC
809 fluxes. At an annual scale the calculated POC fluxes slightly underestimate the measured
810 fluxes (93.1 versus 98.2 mmol m^{-2}). This might results from the minor contribution of full
811 cells other than the diatoms species considered, aggregated material, organic matter sorbed to
812 the exterior of empty cells and faecal fluff that was difficult to enumerate.

813 A scheme of phytoplankton and zooplankton communities succession in naturally-
814 fertilized areas of the Southern Ocean was proposed by Quéguiner (2013). Spring
815 phytoplankton communities are characterized by small, lightly silicified, fast growing diatoms
816 associated with small microphageous copepods. In summer, the phytoplankton community
817 progressively switches toward large, highly silicified, slow growing diatoms resistant to the
818 grazing by large copepods. In this scheme carbon export occurs mostly in end summer
819 through the fall dump. The species succession directly observed in our sediment trap samples
820 differs somewhat to the conceptual model proposed by Quéguiner (2013), although the
821 general patterns are similar. The diatom species exported in spring were *F. kerguelensis*, *T.*
822 *nitzschioides* spp., and small centric species (<20 µm), whilst in summer the comparatively
823 very large (>200 µm) species of *Proboscia* sp., *Rhizosolenia* sp. *and Thalassiothrix antarctica*
824 were observed. However we observe that these species constituting the spring fluxes are
825 exported almost exclusively as empty cells. The abundance of small spherical and ovoid
826 faecal pellet suggests an important role of small copepods in the zooplankton (Yoon et al.,

2001; Wilson et al., 2013), which was corroborated by the finding of dominant *Oithona similis* abundances in the spring mesozooplankton assemblages at station A3 (Carlotti et al., 2015). Therefore, our data suggests that spring export captured by the sediment trap was the remnants of a diatom community subject to efficient grazing and carbon utilization in, or at the basis of, the mixed layer, resulting in a BSi:POC export ratio > 2 (Table 1).

The main difference in our observations and the conceptual scheme of Quéguiner, (2013) is the dominance of *Chaetoceros Hyalochaete* resting spores to diatom export assemblages and their contribution to carbon fluxes out of the mixed layer in summer. Resting spores appear to efficiently bypass the "carbon trap" represented by grazers and might also physically entrain small faecal pellets in their downward flux. In mid-summer, faecal pellet carbon export is dominated by the contribution of cylindrical shapes. This appears to be consistent with an observed shift toward a higher contribution of large copepods and euphausiids to the mesozooplankton community in the mixed layer (Carlotti et al., 2008). However, CRS still dominate the diatom exported assemblage. The corresponding BSi:POC ratio decreases with values between 1 and 2 (Table 1). The fact that there are two discrete resting spore export events might be explained by a mixing event that injected $Si(OH)_4$ into the surface allowing the development of a secondary $Si(OH)_4$ limitation.

In the autumn and winter, diatom fluxes are very low and faecal pellet carbon export is dominated by cylindrical and tabular contributions consistent with a supposed shift to zooplankton communities dominated by large copepods, euphausiids, and salps (Wilson et al., 2013). The low BSi:POC ratios characterizing export at this time suggest that these communities feed primarily suspended particles (in the case of salps) and on micro- and mesozooplankton or small diatoms, although direct measurements of faecal pellet content would be necessary to confirm this.

5 Conclusion

We report the chemical (particulate organic carbon and nitrogen, biogenic silica) and biological (diatom cells and faecal pellets) composition of material exported beneath the winter mixed layer (289 m) in a naturally iron-fertilized area of the Southern Ocean. Annually integrated organic carbon export from the iron-fertilized bloom was low (98 mmol m^{-2}) although biogenic silicon export was significant (114 mmol m^{-2}). *Chaetoceros Hyalochaete* and *Thalassiosira antarctica* resting spores accounted for more than 60 % of the annual POC flux. The high abundance of empty cells and the low contribution of faecal pellets to POC flux (34 %) suggest efficient carbon retention occurs in, or at the base of the mixed layer. We propose that in this HBLE environment, carbon-rich and fast-sinking resting spores bypass the intense grazing pressure otherwise responsible for the rapid attenuation of flux. The seasonal succession of diatom taxa groups was tightly linked to the stoichiometry of the exported material. Several species were identified as primarily "silica sinkers" e.g. *Fragilariopsis kerguelensis* and *Thalassionema nitzschioides* spp. and others as preferential "carbon sinkers" e.g. resting spores of *Chaetoceros Hyalochaete* and *Thalassiosira antarctica*, *Eucampia antarctica* var. *antarctica* and the giant diatom *Thalassiothrix antarctica*. Faecal pellet types described a clear transition from small spherical shapes (small copepods) in spring, larger cylindrical an ellipsoid shapes in summer (euphausiids and large copepods) and large tabular shape (salps) in fall. Their contribution to carbon fluxes increased with the presence of larger shapes.

The change in biological productivity and ocean circulation cannot explain the ~80 ppmv atmospheric pCO_2 difference between the preindustrial era and the last glacial maximum (Archer et al., 2000; Bopp et al., 2003; Kohfeld et al., 2005; Wolff et al., 2006). Nevertheless, a simple switch in 'silica sinker' versus 'carbon sinker' relative abundance would have a drastic effect on carbon sequestration in the Southern Ocean and silicic acid availability at lower latitudes (Sarmiento et al., 2004; Boyd, 2013). The results presented here

emphasize the compelling need for similar studies in other locations of the global Ocean that will allow identification of key ecological vectors that set the magnitude and the stoichiometry of the biological pump.

Acknowledgements

We thank the Captain Bernard Lassiette and his crew during the KEOPS2 mission on the R/V *Marion Dufresne II*. We thank Karine Leblanc and Marine Lasbleiz and three anonymous reviewers for their constructive comments, which helped us to improve the manuscript. This work was supported by the French Research program of INSU-CNRS LEFE-CYBER (Les enveloppes fluides et l'environnement – Cycles biogéochimiques, environnement et ressources), the French ANR (Agence Nationale de la Recherche, SIMI-6 program, ANR-10-BLAN-0614), the French CNES (Centre National d'Etudes Spatiales) and the French Polar Institute IPEV (Institut Polaire Paul-Emile Victor). L. Armand's participation in the KEOPS2 program was supported by an Australian Antarctic Division grant (#3214).

References

Abdi, H., 2010. Partial least squares regression and projection on latent structure regression (PLS Regression). Wiley Interdiscip. Rev. Comput. Stat. 2, 97–106. doi:10.1002/wics.51

Abelmann, A., Gersonde, R., 1991. Biosiliceous particle flux in the Southern Ocean. Mar. Chem., Biochemistry and circulation of water masses in the Southern Ocean International Symposium 35, 503–536. doi:10.1016/S0304-4203(09)90040-8

Allen, C.S., Pike, J., Pudsey, C.J., Leventer, A., 2005. Submillennial variations in ocean conditions during deglaciation based on diatom assemblages from the southwest Atlantic. Paleoceanography 20, PA2012. doi:10.1029/2004PA001055

Aminot, A., Kerouel, R., 2007. Dosage automatique des nutriments dans les eaux marines: méthodes en flux continu. Ifremer, Plouzané, France.

Archer, D., Winguth, A., Lea, D., Mahowald, N., 2000. What caused the glacial/interglacial atmospheric pCO2 cycles? Rev. Geophys. 38, 159–189. doi:10.1029/1999RG000066

Armand, L.K., Cornet-Barthaux, V., Mosseri, J., Quéguiner, B., 2008a. Late summer diatom biomass and community structure on and around the naturally iron-fertilised Kerguelen Plateau in the Southern Ocean. Deep Sea Res. Part II Top. Stud. Oceanogr., KEOPS: Kerguelen Ocean and Plateau compared Study 55, 653–676. doi:10.1016/j.dsr2.2007.12.031

Armand, L.K., Crosta, X., Quéguiner, B., Mosseri, J., Garcia, N., 2008b. Diatoms preserved in surface sediments of the northeastern Kerguelen Plateau. Deep Sea Res. Part II Top. Stud. Oceanogr. 55, 677–692. doi:10.1016/j.dsr2.2007.12.032

Armand, L.K., Crosta, X., Romero, O., Pichon, J.-J., 2005. The biogeography of major diatom taxa in Southern Ocean sediments: 1. Sea ice related species. Palaeogeogr. Palaeoclimatol. Palaeoecol. 223, 93–126. doi:10.1016/j.palaeo.2005.02.015

Arrigo, K.R., Worthen, D., Schnell, A., Lizotte, M.P., 1998. Primary production in Southern Ocean waters. J. Geophys. Res. Oceans 103, 15587–15600. doi:10.1029/98JC00930

Assmy, P., Smetacek, V., Montresor, M., Klaas, C., Henjes, J., Strass, V.H., Arrieta, J.M., Bathmann, U., Berg, G.M., Breitbarth, E., Cisewski, B., Friedrichs, L., Fuchs, N., Herndl, G.J., Jansen, S., Krägefsky, S., Latasa, M., Peeken, I., Röttgers, R., Scharek, R., Schüller, S.E., Steigenberger, S., Webb, A., Wolf-Gladrow, D., 2013. Thick-shelled, grazer-protected diatoms decouple ocean carbon and silicon cycles in the iron-limited Antarctic Circumpolar Current. Proc. Natl. Acad. Sci. 110, 20633–20638. doi:10.1073/pnas.1309345110

Baker, E.T., Milburn, H.B., Tennant, D.A., 1988. Field assessment of sediment trap efficiency under varying flow conditions. J. Mar. Res. 46, 573–592. doi:10.1357/002224088785113522

Bao, R., Stigter, H.D., Weering, T.C.E.V., 2000. Diatom fluxes in surface sediments of the Goban Spur continental margin, NE Atlantic Ocean. J. Micropalaeontology 19, 123–131. doi:10.1144/jm.19.2.123

Blain, S., Quéguiner, B., Armand, L., Belviso, S., Bombled, B., Bopp, L., Bowie, A., Brunet, C., Brussaard, C., Carlotti, F., Christaki, U., Corbière, A., Durand, I., Ebersbach, F., Fuda, J.-L., Garcia, N., Gerringa, L., Griffiths, B., Guigue, C., Guillerm, C., Jacquet, S., Jeandel, C., Laan, P., Lefèvre, D., Lo Monaco, C., Malits, A., Mosseri, J., Obernosterer, I., Park, Y.-H., Picheral, M., Pondaven, P., Remenyi, T., Sandroni, V., Sarthou, G., Savoye, N., Scouarnec, L., Souhaut, M., Thuiller, D., Timmermans, K., Trull, T., Uitz, J., van Beek, P., Veldhuis, M., Vincent, D., Viollier, E., Vong, L., Wagener, T., 2007. Effect of natural iron fertilization on carbon sequestration in the Southern Ocean. Nature 446, 1070–1074. doi:10.1038/nature05700

Blain, S., Renaut, S., Xing, X., Claustre, H., Guinet, C., 2013. Instrumented elephant seals reveal the seasonality in chlorophyll and light-mixing regime in the iron-fertilized Southern Ocean. Geophys. Res. Lett. 40, 6368–6372. doi:10.1002/2013GL058065

Blain, S., Tréguer, P., Belviso, S., Bucciarelli, E., Denis, M., Desabre, S., Fiala, M., Martin Jézéquel, V., Le Fèvre, J., Mayzaud, P., Marty, J.-C., Razouls, S., 2001. A biogeochemical study of the island mass effect in the context of the iron hypothesis: Kerguelen Islands, Southern Ocean. Deep Sea Res. Part Oceanogr. Res. Pap. 48, 163–187. doi:10.1016/S0967-0637(00)00047-9

Bodungen, B. von, 1986. Phytoplankton growth and krill grazing during spring in the Bransfield Strait, Antarctica — Implications from sediment trap collections. Polar Biol. 6, 153–160. doi:10.1007/BF00274878

Bopp, L., Kohfeld, K.E., Le Quéré, C., Aumont, O., 2003. Dust impact on marine biota and atmospheric CO2 during glacial periods. Paleoceanography 18, 1046. doi:10.1029/2002PA000810

Bowie, A.R., van der Merwe, P., Quéroué, F., Trull, T., Fourquez, M., Planchon, F., Sarthou, G., Chever, F., Townsend, A.T., Obernosterer, I., Sallée, J.-B., Blain, S., 2014. Iron budgets for three distinct biogeochemical sites around the Kerguelen archipelago (Southern Ocean) during the natural fertilisation experiment KEOPS-2. Biogeosciences Discuss 11, 17861–17923. doi:10.5194/bgd-11-17861-2014

Boyd, P.W., 2013. Diatom traits regulate Southern Ocean silica leakage. Proc. Natl. Acad. Sci. 110, 20358–20359. doi:10.1073/pnas.1320327110

Brzezinski, M.A., 1985. The Si:C:N ratio of marine diatoms: interspecific variability and the effect of some environmental variables. J. Phycol. 21, 347–357. doi:10.1111/j.0022-3646.1985.00347.x

Brzezinski, M.A., Pride, C.J., Franck, V.M., Sigman, D.M., Sarmiento, J.L., Matsumoto, K., Gruber, N., Rau, G.H., Coale, K.H., 2002. A switch from Si(OH)4 to NO3− depletion in the glacial Southern Ocean. Geophys. Res. Lett. 29. doi:10.1029/2001GL014349

Buesseler, K.O., 1998. The decoupling of production and particulate export in the surface ocean. Glob. Biogeochem. Cycles 12, 297–310. doi:10.1029/97GB03366

Buesseler, K.O., Antia, A.N., Chen, M., Fowler, S.W., Gardner, W.D., Gustafsson, Ö., Harada, K., Michaels, A.F., Rutgers v. d. Loeff, M., Sarin, M., Steinberg, D.K., Trull, T., 2007. An assessment of the use of sediment traps for estimating upper ocean particle fluxes. J. Mar. Res. 65, 345–416.

Buesseler, K.O., Steinberg, D.K., Michaels, A.F., Johnson, R.J., Andrews, J.E., Valdes, J.R., Price, J.F., 2000. A comparison of the quantity and composition of material caught in a neutrally buoyant versus surface-tethered sediment trap. Deep Sea Res. Part Oceanogr. Res. Pap. 47, 277–294. doi:10.1016/S0967-0637(99)00056-4

Burd, A.B., Jackson, G.A., 2009. Particle Aggregation. Annu. Rev. Mar. Sci. 1, 65–90. doi:10.1146/annurev.marine.010908.163904

Carlotti, F., Jouandet, M.-P., Nowaczyk, A., Harmelin-Vivien, M., Lefèvre, D., Guillou, G., Zhu, Y., Zhou, M., 2015. Mesozooplankton structure and functioning during the onset of the Kerguelen phytoplankton bloom during the Keops2 survey. Biogeosciences Discuss 12, 2381–2427. doi:10.5194/bgd-12-2381-2015

Carlotti, F., Thibault-Botha, D., Nowaczyk, A., Lefèvre, D., 2008. Zooplankton community structure, biomass and role in carbon fluxes during the second half of a phytoplankton bloom in the eastern sector of the Kerguelen Shelf (January–February 2005). Deep Sea Res. Part II Top. Stud. Oceanogr., KEOPS: Kerguelen Ocean and Plateau compared Study 55, 720–733. doi:10.1016/j.dsr2.2007.12.010

Cavan, E.L., Le Moigne, F. a. c., Poulton, A.J., Tarling, G.A., Ward, P., Daniels, C.J., Fragoso, G., Sanders, R.J., 2015. Zooplankton fecal pellets control the attenuation of particulate organic carbon flux in the Scotia Sea, Southern Ocean. Geophys. Res. Lett. 2014GL062744. doi:10.1002/2014GL062744

Chang, A.S., Bertram, M.A., Ivanochko, T., Calvert, S.E., Dallimore, A., Thomson, R.E., 2013. Annual record of particle fluxes, geochemistry and diatoms in Effingham Inlet, British Columbia, Canada, and the impact of the 1999 La Niña event. Mar. Geol. 337, 20–34. doi:10.1016/j.margeo.2013.01.003

Christaki, U., Lefèvre, D., Georges, C., Colombet, J., Catala, P., Courties, C., Sime-Ngando, T., Blain, S., Obernosterer, I., 2014. Microbial food web dynamics during spring phytoplankton blooms in the naturally iron-fertilized Kerguelen area (Southern Ocean). Biogeosciences 11, 6739–6753. doi:10.5194/bg-11-6739-2014

Closset, I., Lasbleiz, M., Leblanc, K., Quéguiner, B., Cavagna, A.-J., Elskens, M., Navez, J., Cardinal, D., 2014. Seasonal evolution of net and regenerated silica production around a natural Fe-fertilized area in the Southern Ocean estimated with Si isotopic approaches. Biogeosciences 11, 5827–5846. doi:10.5194/bg-11-5827-2014

997 Cornet-Barthaux, V., Armand, L., Quguiner, B., 2007. Biovolume and biomass estimates of key
998 diatoms in the Southern Ocean. Aquat. Microb. Ecol. 48, 295–308. doi:10.3354/ame048295
999 Crawford, R., 1995. The role of sex in the sedimentation of a marine diatom bloom. Limnol.
1000 Oceanogr. 40, 200–204.
1001 Crosta, X., Pichon, J.-J., Labracherie, M., 1997. Distribution of Chaetoceros resting spores in modern
1002 peri-Antarctic sediments. Mar. Micropaleontol. 29, 283–299. doi:10.1016/S0377-
1003 8398(96)00033-3
1004 Davison, P.C., Checkley Jr., D.M., Koslow, J.A., Barlow, J., 2013. Carbon export mediated by
1005 mesopelagic fishes in the northeast Pacific Ocean. Prog. Oceanogr. 116, 14–30.
1006 doi:10.1016/j.pocean.2013.05.013
1007 DeMaster, D.J., 1981. The supply and accumulation of silica in the marine environment. Geochim.
1008 Cosmochim. Acta 45, 1715–1732. doi:10.1016/0016-7037(81)90006-5
1009 Doucette, G.J., Fryxell, G.A., 1983. Thalassiosira antarctica: vegetative and resting stage chemical
1010 composition of an ice-related marine diatom. Mar. Biol. 78, 1–6. doi:10.1007/BF00392964
1011 Dubischar, C.D., Bathmann, U.V., 2002. The occurrence of faecal material in relation to different
1012 pelagic systems in the Southern Ocean and its importance for vertical flux. Deep Sea Res. Part
1013 II Top. Stud. Oceanogr., The Southern Ocean II: Climatic Changes and the Cycle of Carbon
1014 49, 3229–3242. doi:10.1016/S0967-0645(02)00080-2
1015 Dunbar, R.B., 1984. Sediment trap experiments on the Antarctic continental margin. Antarct. J. US
1016 70–71.
1017 Dutkiewicz, S., Follows, M.J., Parekh, P., 2005. Interactions of the iron and phosphorus cycles: A
1018 three-dimensional model study. Glob. Biogeochem. Cycles 19, GB1021.
1019 doi:10.1029/2004GB002342
1020 Ebersbach, F., Assmy, P., Martin, P., Schulz, I., Wolzenburg, S., Nöthig, E.-M., 2014. Particle flux
1021 characterisation and sedimentation patterns of protistan plankton during the iron fertilisation
1022 experiment LOHAFEX in the Southern Ocean. Deep Sea Res. Part Oceanogr. Res. Pap. 89,
1023 94–103. doi:10.1016/j.dsr.2014.04.007
1024 Ebersbach, F., Trull, T.W., 2008. Sinking particle properties from polyacrylamide gels during the
1025 KErguelen Ocean and Plateau compared Study (KEOPS): Zooplankton control of carbon
1026 export in an area of persistent natural iron inputs in the Southern Ocean. Limnol. Oceanogr.
1027 53, 212–224. doi:10.4319/lo.2008.53.1.0212
1028 Ebersbach, F., Trull, T.W., Davies, D.M., Bray, S.G., 2011. Controls on mesopelagic particle fluxes in
1029 the Sub-Antarctic and Polar Frontal Zones in the Southern Ocean south of Australia in
1030 summer—Perspectives from free-drifting sediment traps. Deep Sea Res. Part II Top. Stud.
1031 Oceanogr. 58, 2260–2276. doi:10.1016/j.dsr2.2011.05.025
1032 Fischer, G., Fütterer, D., Gersonde, R., Honjo, S., Ostermann, D., Wefer, G., 1988. Seasonal
1033 variability of particle flux in the Weddell Sea and its relation to ice cover. Nature 335, 426–
1034 428. doi:10.1038/335426a0
1035 Fischer, G., Gersonde, R., Wefer, G., 2002. Organic carbon, biogenic silica and diatom fluxes in the
1036 marginal winter sea-ice zone and in the Polar Front Region: interannual variations and
1037 differences in composition. Deep Sea Res. Part II Top. Stud. Oceanogr. 49, 1721–1745.
1038 doi:10.1016/S0967-0645(02)00009-7
1039 Fransz, H.G., Gonzalez, S.R., 1995. The production of Oithona similis (Copepoda: Cyclopoida) in the
1040 Southern Ocean. ICES J. Mar. Sci. J. Cons. 52, 549–555. doi:10.1016/1054-3139(95)80069-7
1041 Garrison, D.L., 1981. Monterey Bay Phytoplankton. II. Resting Spore Cycles in Coastal Diatom
1042 Populations. J. Plankton Res. 3, 137–156. doi:10.1093/plankt/3.1.137
1043 Gersonde, R., Zielinski, U., 2000. The reconstruction of late Quaternary Antarctic sea-ice
1044 distribution—the use of diatoms as a proxy for sea-ice. Palaeogeogr. Palaeoclimatol.
1045 Palaeoecol. 162, 263–286. doi:10.1016/S0031-0182(00)00131-0
1046 Gleiber, M.R., Steinberg, D.K., Ducklow, H.W., 2012. Time series of vertical flux of zooplankton
1047 fecal pellets on the continental shelf of the western Antarctic Peninsula. Mar. Ecol. Prog. Ser.
1048 471, 23–36. doi:10.3354/meps10021
1049 Gomi, Y., Fukuchi, M., Taniguchi, A., 2010. Diatom assemblages at subsurface chlorophyll maximum
1050 layer in the eastern Indian sector of the Southern Ocean in summer. J. Plankton Res. 32, 1039–
1051 1050. doi:10.1093/plankt/fbq031

Gonzalez, H.E., Smetacek, V., 1994. The possible role of the cyclopoid copepod Oithona in retarding vertical flux of zooplankton faecal material. Mar. Ecol.-Prog. Ser. 113, 233–246.
Grigorov, I., Rigual-Hernandez, A.S., Honjo, S., Kemp, A.E.S., Armand, L.K., 2014a. Settling fluxes of diatoms to the interior of the Antarctic circumpolar current along 170 °W. Deep Sea Res. Part Oceanogr. Res. Pap. 93, 1–13. doi:10.1016/j.dsr.2014.07.008
Grigorov, I., Rigual-Hernandez, A.S., Honjo, S., Kemp, A.E.S., Armand, L.K., 2014b. Settling fluxes of diatoms to the interior of the Antarctic circumpolar current along 170 °W. Deep Sea Res. Part Oceanogr. Res. Pap. 93, 1–13. doi:10.1016/j.dsr.2014.07.008
Grimm, K.A., Lange, C.B., Gill, A.S., 1996. Biological forcing of hemipelagic sedimentary laminae; evidence from ODP Site 893, Santa Barbara Basin, California. J. Sediment. Res. 66, 613–624. doi:10.1306/D42683C4-2B26-11D7-8648000102C1865D
Hasle, G.R., Syvertsen, E.E., 1997. Chapter 2 - Marine Diatoms, in: Tomas, C.R. (Ed.), Identifying Marine Phytoplankton. Academic Press, San Diego, pp. 5–385.
Hillebrand, H., Dürselen, C.-D., Kirschtel, D., Pollingher, U., Zohary, T., 1999. Biovolume Calculation for Pelagic and Benthic Microalgae. J. Phycol. 35, 403–424. doi:10.1046/j.1529-8817.1999.3520403.x
Holm-Hansen, O., Kahru, M., Hewes, C.D., Kawaguchi, S., Kameda, T., Sushin, V.A., Krasovski, I., Priddle, J., Korb, R., Hewitt, R.P., Mitchell, B.G., 2004. Temporal and spatial distribution of chlorophyll-a in surface waters of the Scotia Sea as determined by both shipboard measurements and satellite data. Deep Sea Res. Part II Top. Stud. Oceanogr. 51, 1323–1331. doi:10.1016/j.dsr2.2004.06.004
Holzer, M., Primeau, F.W., DeVries, T., Matear, R., 2014. The Southern Ocean silicon trap: Data-constrained estimates of regenerated silicic acid, trapping efficiencies, and global transport paths. J. Geophys. Res. Oceans 119, 313–331. doi:10.1002/2013JC009356
Howard, A.G., Coxhead, A.J., Potter, I.A., Watt, A.P., 1986. Determination of dissolved aluminium by the micelle-enhanced fluorescence of its lumogallion complex. Analyst 111, 1379–1382. doi:10.1039/AN9861101379
Hutchins, D.A., Bruland, K.W., 1998. Iron-limited diatom growth and Si:N uptake ratios in a coastal upwelling regime. Nature 393, 561–564. doi:10.1038/31203
Ichinomiya, M., Gomi, Y., Nakamachi, M., Honda, M., Fukuchi, M., Taniguchi, A., 2008. Temporal variations in the abundance and sinking flux of diatoms under fast ice in summer near Syowa Station, East Antarctica. Polar Sci. 2, 33–40. doi:10.1016/j.polar.2008.01.001
Jackson, G.A., Burd, A.B., 2001. A model for the distribution of particle flux in the mid-water column controlled by subsurface biotic interactions. Deep Sea Res. Part II Top. Stud. Oceanogr., The US JGOFS Synthesis and Modeling Project: Phase 1 49, 193–217. doi:10.1016/S0967-0645(01)00100-X
Jackson, G.A., Waite, A.M., Boyd, P.W., 2005. Role of algal aggregation in vertical carbon export during SOIREE and in other low biomass environments. Geophys. Res. Lett. 32, L13607. doi:10.1029/2005GL023180
Jin, X., Gruber, N., Dunne, J.P., Sarmiento, J.L., Armstrong, R.A., 2006. Diagnosing the contribution of phytoplankton functional groups to the production and export of particulate organic carbon, CaCO3, and opal from global nutrient and alkalinity distributions. Glob. Biogeochem. Cycles 20, GB2015. doi:10.1029/2005GB002532
Jouandet, M.P., Blain, S., Metzl, N., Brunet, C., Trull, T.W., Obernosterer, I., 2008. A seasonal carbon budget for a naturally iron-fertilized bloom over the Kerguelen Plateau in the Southern Ocean. Deep Sea Res. Part II Top. Stud. Oceanogr., KEOPS: Kerguelen Ocean and Plateau compared Study 55, 856–867. doi:10.1016/j.dsr2.2007.12.037
Jouandet, M.-P., Jackson, G.A., Carlotti, F., Picheral, M., Stemmann, L., Blain, S., 2014. Rapid formation of large aggregates during the spring bloom of Kerguelen Island: observations and model comparisons. Biogeosciences 11, 4393–4406. doi:10.5194/bg-11-4393-2014
Jouandet, M.-P., Trull, T.W., Guidi, L., Picheral, M., Ebersbach, F., Stemmann, L., Blain, S., 2011. Optical imaging of mesopelagic particles indicates deep carbon flux beneath a natural iron-fertilized bloom in the Southern Ocean. Limnol. Oceanogr. 56, 1130–1140. doi:10.4319/lo.2011.56.3.1130

Kato, M., Tanimura, Y., Matsuoka, K., Fukusawa, H., 2003. Planktonic diatoms from sediment traps in Omura Bay, western Japan with implications for ecological and taphonomic studies of coastal marine environments. Quat. Int. 105, 25–31. doi:10.1016/S1040-6182(02)00147-7

Kemp, A.E.., Pike, J., Pearce, R.B., Lange, C.B., 2000. The "Fall dump" — a new perspective on the role of a "shade flora" in the annual cycle of diatom production and export flux. Deep Sea Res. Part II Top. Stud. Oceanogr. 47, 2129–2154. doi:10.1016/S0967-0645(00)00019-9

Kemp, A.E.S., Villareal, T.A., 2013. High diatom production and export in stratified waters – A potential negative feedback to global warming. Prog. Oceanogr. 119, 4–23. doi:10.1016/j.pocean.2013.06.004

Kohfeld, K.E., Quéré, C.L., Harrison, S.P., Anderson, R.F., 2005. Role of Marine Biology in Glacial-Interglacial CO2 Cycles. Science 308, 74–78. doi:10.1126/science.1105375

Kopczynska, E.E., Dehairs, F., Elskens, M., Wright, S., 2001. Phytoplankton and microzooplankton variability between the Subtropical and Polar Fronts south of Australia: Thriving under regenerative and new production in late summer. J. Geophys. Res. Oceans 106, 31597–31609. doi:10.1029/2000JC000278

Kuwata, A., Hama, T., Takahashi, M., 1993. Ecophysiological characterization of two life forms, resting spores and resting cells, of a marine planktonic diatom. Mar. Ecol. Prog. Ser. 102, 245–255.

Kuwata, A., Tsuda, A., 2005. Selection and viability after ingestion of vegetative cells, resting spores and resting cells of the marine diatom, Chaetoceros pseudocurvisetus, by two copepods. J. Exp. Mar. Biol. Ecol. 322, 143–151. doi:10.1016/j.jembe.2005.02.013

Lampitt, R.S., Boorman, B., Brown, L., Lucas, M., Salter, I., Sanders, R., Saw, K., Seeyave, S., Thomalla, S.J., Turnewitsch, R., 2008. Particle export from the euphotic zone: Estimates using a novel drifting sediment trap, 234Th and new production. Deep Sea Res. Part Oceanogr. Res. Pap. 55, 1484–1502. doi:10.1016/j.dsr.2008.07.002

Lampitt, R.S., Noji, T., Bodungen, B. von, 1990. What happens to zooplankton faecal pellets? Implications for material flux. Mar. Biol. 104, 15–23. doi:10.1007/BF01313152

Lampitt, R.S., Salter, I., Johns, D., 2009. Radiolaria: Major exporters of organic carbon to the deep ocean. Glob. Biogeochem. Cycles 23, GB1010. doi:10.1029/2008GB003221

Lam, P.J., Bishop, J.K.B., 2007. High biomass, low export regimes in the Southern Ocean. Deep Sea Res. Part II Top. Stud. Oceanogr. 54, 601–638. doi:10.1016/j.dsr2.2007.01.013

Lam, P.J., Doney, S.C., Bishop, J.K.B., 2011. The dynamic ocean biological pump: Insights from a global compilation of particulate organic carbon, CaCO3, and opal concentration profiles from the mesopelagic. Glob. Biogeochem. Cycles 25, GB3009. doi:10.1029/2010GB003868

Lange, 1997. Sedimentation patterns of diatoms, radiolarians, and silicoflagellates in Santa Barbara Basin, California. Calif. Coop. Ocean. Fish. Investig. Rep. 38, 161–170.

Lange, C.B., Weinheimer, A.L., Reid, F.M.H., Thunell, R.C., 1997. Sedimentation patterns of diatoms, radiolarians, and silicoflagellates in Santa Barbara Basin, California. Calif. Coop. Ocean. Fish. Investig. Rep. 38, 161–170.

Lasbleiz, M., Leblanc, K., Blain, S., Ras, J., Cornet-Barthaux, V., Hélias Nunige, S., Quéguiner, B., 2014. Pigments, elemental composition (C, N, P, and Si), and stoichiometry of particulate matter in the naturally iron fertilized region of Kerguelen in the Southern Ocean. Biogeosciences 11, 5931–5955. doi:10.5194/bg-11-5931-2014

Laurenceau, E.C., Trull, T.W., Davies, D.M., Bray, S.G., Doran, J., Planchon, F., Carlotti, F., Jouandet, M.-P., Cavagna, A.-J., Waite, A.M., Blain, S., 2014. The relative importance of phytoplankton aggregates and zooplankton fecal pellets to carbon export: insights from free-drifting sediment trap deployments in naturally iron-fertilised waters near the Kerguelen plateau. Biogeosciences Discuss 11, 13623–13673. doi:10.5194/bgd-11-13623-2014

Legendre, P., Dr, L.F.J.L., 1998. Numerical Ecology, Édition : 2. ed. Elsevier Science, Amsterdam ; New York.

Leventer, A., 1991. Sediment trap diatom assemblages from the northern Antarctic Peninsula region. Deep Sea Res. Part Oceanogr. Res. Pap. 38, 1127–1143. doi:10.1016/0198-0149(91)90099-2

Leventer, A., Dunbar, R.B., 1987. Diatom flux in McMurdo Sound, Antarctica. Mar. Micropaleontol. 12, 49–64. doi:10.1016/0377-8398(87)90013-2

Lopes, C., Mix, A.C., Abrantes, F., 2006. Diatoms in northeast Pacific surface sediments as paleoceanographic proxies. Mar. Micropaleontol. 60, 45–65. doi:10.1016/j.marmicro.2006.02.010

Madin, L.P., 1982. Production, composition and sedimentation of salp fecal pellets in oceanic waters. Mar. Biol. 67, 39–45. doi:10.1007/BF00397092

Maiti, K., Charette, M.A., Buesseler, K.O., Kahru, M., 2013. An inverse relationship between production and export efficiency in the Southern Ocean. Geophys. Res. Lett. 40, 1557–1561. doi:10.1002/grl.50219

Martin, J.H., Gordon, R.M., Fitzwater, S.E., 1990. Iron in Antarctic waters. Nature 345, 156–158. doi:10.1038/345156a0

Matsumoto, K., Sarmiento, J.L., Brzezinski, M.A., 2002. Silicic acid leakage from the Southern Ocean: A possible explanation for glacial atmospheric pCO2. Glob. Biogeochem. Cycles 16, 5–1. doi:10.1029/2001GB001442

McQuoid, M.R., Hobson, L.A., 1996. Diatom Resting Stages. J. Phycol. 32, 889–902. doi:10.1111/j.0022-3646.1996.00889.x

Menden-Deuer, S., Lessard, E.J., 2000. Carbon to volume relationships for dinoflagellates, diatoms, and other protist plankton. Limnol. Oceanogr. 45, 569–579. doi:10.4319/lo.2000.45.3.0569

Moore, C.M., Mills, M.M., Arrigo, K.R., Berman-Frank, I., Bopp, L., Boyd, P.W., Galbraith, E.D., Geider, R.J., Guieu, C., Jaccard, S.L., Jickells, T.D., La Roche, J., Lenton, T.M., Mahowald, N.M., Marañón, E., Marinov, I., Moore, J.K., Nakatsuka, T., Oschlies, A., Saito, M.A., Thingstad, T.F., Tsuda, A., Ulloa, O., 2013. Processes and patterns of oceanic nutrient limitation. Nat. Geosci. 6, 701–710. doi:10.1038/ngeo1765

Moore, J.K., Doney, S.C., Glover, D.M., Fung, I.Y., 2001. Iron cycling and nutrient-limitation patterns in surface waters of the World Ocean. Deep Sea Res. 49, 463–507. doi:10.1016/S0967-0645(01)00109-6

Mortlock, R.A., Froelich, P.N., 1989. A simple method for the rapid determination of biogenic opal in pelagic marine sediments. Deep Sea Res. Part Oceanogr. Res. Pap. 36, 1415–1426. doi:10.1016/0198-0149(89)90092-7

Mosseri, J., Quéguiner, B., Armand, L., Cornet-Barthaux, V., 2008. Impact of iron on silicon utilization by diatoms in the Southern Ocean: A case study of Si/N cycle decoupling in a naturally iron-enriched area. Deep Sea Res. Part II Top. Stud. Oceanogr., KEOPS: Kerguelen Ocean and Plateau compared Study 55, 801–819. doi:10.1016/j.dsr2.2007.12.003

Nelson, D.M., Brzezinski, M.A., Sigmon, D.E., Franck, V.M., 2001. A seasonal progression of Si limitation in the Pacific sector of the Southern Ocean. Deep Sea Res. Part II Top. Stud. Oceanogr. 48, 3973–3995. doi:10.1016/S0967-0645(01)00076-5

Nelson, D.M., Tréguer, P., Brzezinski, M.A., Leynaert, A., Quéguiner, B., 1995. Production and dissolution of biogenic silica in the ocean: Revised global estimates, comparison with regional data and relationship to biogenic sedimentation. Glob. Biogeochem. Cycles 9, 359–372. doi:10.1029/95GB01070

Obernosterer, I., Christaki, U., Lefèvre, D., Catala, P., Van Wambeke, F., Lebaron, P., 2008. Rapid bacterial mineralization of organic carbon produced during a phytoplankton bloom induced by natural iron fertilization in the Southern Ocean. Deep Sea Res. Part II Top. Stud. Oceanogr. 55, 777–789. doi:10.1016/j.dsr2.2007.12.005

Oku, O., Kamatani, A., 1997. Resting spore formation of the marine planktonic diatom Chaetoceros anastomosans induced by high salinity and nitrogen depletion. Mar. Biol. 127, 515–520. doi:10.1007/s002270050040

Onodera, J., Watanabe, E., Harada, N., Honda, M.C., 2014. Diatom flux reflects water-mass conditions on the southern Northwind Abyssal Plain, Arctic Ocean. Biogeosciences Discuss 11, 15215–15250. doi:10.5194/bgd-11-15215-2014

Park, J., Oh, I.-S., Kim, H.-C., Yoo, S., 2010. Variability of SeaWiFs chlorophyll-a in the southwest Atlantic sector of the Southern Ocean: Strong topographic effects and weak seasonality. Deep Sea Res. Part Oceanogr. Res. Pap. 57, 604–620. doi:10.1016/j.dsr.2010.01.004

Park, Y.-H., Durand, I., Kestenare, E., Rougier, G., Zhou, M., d' Ovidio, F., Cotté, C., Lee, J.-H., 2014. Polar Front around the Kerguelen Islands: An up-to-date determination and associated

circulation of surface/subsurface waters. J. Geophys. Res. Oceans 119, 6575–6592. doi:10.1002/2014JC010061

Park, Y.-H., Roquet, F., Durand, I., Fuda, J.-L., 2008. Large-scale circulation over and around the Northern Kerguelen Plateau. Deep Sea Res. Part II Top. Stud. Oceanogr. 55, 566–581. doi:10.1016/j.dsr2.2007.12.030

Parslow, J.S., Boyd, P.W., Rintoul, S.R., Griffiths, F.B., 2001. A persistent subsurface chlorophyll maximum in the Interpolar Frontal Zone south of Australia: Seasonal progression and implications for phytoplankton-light-nutrient interactions. J. Geophys. Res. Oceans 106, 31543–31557. doi:10.1029/2000JC000322

Pilskaln, C.H., Manganini, S.J., Trull, T.W., Armand, L., Howard, W., Asper, V.L., Massom, R., 2004. Geochemical particle fluxes in the Southern Indian Ocean seasonal ice zone: Prydz Bay region, East Antarctica. Deep Sea Res. Part Oceanogr. Res. Pap. 51, 307–332. doi:10.1016/j.dsr.2003.10.010

Pinkerton, M.H., Smith, A.N.H., Raymond, B., Hosie, G.W., Sharp, B., Leathwick, J.R., Bradford-Grieve, J.M., 2010. Spatial and seasonal distribution of adult Oithona similis in the Southern Ocean: Predictions using boosted regression trees. Deep Sea Res. Part Oceanogr. Res. Pap. 57, 469–485. doi:10.1016/j.dsr.2009.12.010

Pollard, R.., Lucas, M.., Read, J.., 2002. Physical controls on biogeochemical zonation in the Southern Ocean. Deep Sea Res. Part II Top. Stud. Oceanogr. 49, 3289–3305. doi:10.1016/S0967-0645(02)00084-X

Primeau, F.W., Holzer, M., DeVries, T., 2013. Southern Ocean nutrient trapping and the efficiency of the biological pump. J. Geophys. Res. Oceans 118, 2547–2564. doi:10.1002/jgrc.20181

Quéguiner, B., 2013. Iron fertilization and the structure of planktonic communities in high nutrient regions of the Southern Ocean. Deep Sea Res. Part II Top. Stud. Oceanogr. 90, 43–54. doi:10.1016/j.dsr2.2012.07.024

Ragueneau, O., Savoye, N., Del Amo, Y., Cotten, J., Tardiveau, B., Leynaert, A., 2005. A new method for the measurement of biogenic silica in suspended matter of coastal waters: using Si:Al ratios to correct for the mineral interference. Cont. Shelf Res. 25, 697–710. doi:10.1016/j.csr.2004.09.017

Ragueneau, O., Schultes, S., Bidle, K., Claquin, P., Moriceau, B., 2006. Si and C interactions in the world ocean: Importance of ecological processes and implications for the role of diatoms in the biological pump. Glob. Biogeochem. Cycles 20, GB4S02. doi:10.1029/2006GB002688

Rembauville, M., Salter, I., Leblond, N., Gueneugues, A., Blain, S., 2014. Export fluxes in a naturally fertilized area of the Southern Ocean, the Kerguelen Plateau: seasonal dynamic reveals long lags and strong attenuation of particulate organic carbon flux (Part 1). Biogeosciences Discuss 11, 17043–17087. doi:10.5194/bgd-11-17043-2014

Richardson, K., Visser, A.W., Pedersen, F.B., 2000. Subsurface phytoplankton blooms fuel pelagic production in the North Sea. J. Plankton Res. 22, 1663–1671. doi:10.1093/plankt/22.9.1663

Rigual-Hernández, A.S., Trull, T.W., Bray, S.G., Closset, I., Armand, L.K., 2015. Seasonal dynamics in diatom and particulate export fluxes to the deep sea in the Australian sector of the southern Antarctic Zone. J. Mar. Syst. 142, 62–74. doi:10.1016/j.jmarsys.2014.10.002

Romero, O.E., Armand, L., 2010. Marine diatoms as indicators of modern changes in oceanographic conditions. In: 2nd Edition The Diatoms: Applications for the Environmental and Earth Sciences,. Camb. Univ. Press 373–400.

Romero, O.E., Fischer, G., Lange, C.B., Wefer, G., 2000. Siliceous phytoplankton of the western equatorial Atlantic: sediment traps and surface sediments. Deep Sea Res. Part II Top. Stud. Oceanogr. 47, 1939–1959. doi:10.1016/S0967-0645(00)00012-6

Romero, O.E., Lange, C.B., Fisher, G., Treppke, U.F., Wefer, G., 1999. Variability in export prodution documented by downward fluxes and species composition of marine planktonic diatoms: observations from the tropical and equatorial Atlantic., in: The Use of Proxies in Paleoceanography, Examples from the South Atlantic. Heidelberg, Berlin, pp. 365–392.

Rynearson, T.A., Richardson, K., Lampitt, R.S., Sieracki, M.E., Poulton, A.J., Lyngsgaard, M.M., Perry, M.J., 2013. Major contribution of diatom resting spores to vertical flux in the sub-polar North Atlantic. Deep Sea Res. Part Oceanogr. Res. Pap. 82, 60–71. doi:10.1016/j.dsr.2013.07.013

Sackett, O., Armand, L., Beardall, J., Hill, R., Doblin, M., Connelly, C., Howes, J., Stuart, B., Ralph, P., Heraud, P., 2014. Taxon-specific responses of Southern Ocean diatoms to Fe enrichment revealed by synchrotron radiation FTIR microspectroscopy. Biogeosciences 11, 5795–5808. doi:10.5194/bg-11-5795-2014

Sallée, J.-B., Matear, R.J., Rintoul, S.R., Lenton, A., 2012. Localized subduction of anthropogenic carbon dioxide in the Southern Hemisphere oceans. Nat. Geosci. 5, 579–584. doi:10.1038/ngeo1523

Salter, I., Kemp, A.E.S., Moore, C.M., Lampitt, R.S., Wolff, G.A., Holtvoeth, J., 2012. Diatom resting spore ecology drives enhanced carbon export from a naturally iron-fertilized bloom in the Southern Ocean. Glob. Biogeochem. Cycles 26, GB1014. doi:10.1029/2010GB003977

Salter, I., Lampitt, R.S., Sanders, R., Poulton, A., Kemp, A.E.S., Boorman, B., Saw, K., Pearce, R., 2007. Estimating carbon, silica and diatom export from a naturally fertilised phytoplankton bloom in the Southern Ocean using PELAGRA: A novel drifting sediment trap. Deep Sea Res. Part II Top. Stud. Oceanogr., The Crozet Natural Iron Bloom and Export Experiment CROZEX 54, 2233–2259. doi:10.1016/j.dsr2.2007.06.008

Salter, I., Schiebel, R., Ziveri, P., Movellan, A., Lampitt, R., Wolff, G.A., 2014. Carbonate counter pump stimulated by natural iron fertilization in the Polar Frontal Zone. Nat. Geosci. 7, 885–889. doi:10.1038/ngeo2285

Sancetta, C., 1995. Diatoms in the Gulf of California: Seasonal flux patterns and the sediment record for the last 15,000 years. Paleoceanography 10, 67–84. doi:10.1029/94PA02796

Sanders, J.G., Cibik, S.J., 1985. Reduction of growth rate and resting spore formation in a marine diatom exposed to low levels of cadmium. Mar. Environ. Res. 16, 165–180. doi:10.1016/0141-1136(85)90136-9

Sarmiento, J.L., Gruber, N., Brzezinski, M.A., Dunne, J.P., 2004. High-latitude controls of thermocline nutrients and low latitude biological productivity. Nature 427, 56–60. doi:10.1038/nature02127

Schnack-Schiel, S.B., Isla, E., 2005. The role of zooplankton in the pelagic-benthic coupling of the Southern Ocean. Sci. Mar. 39–55.

Smetacek, V., Assmy, P., Henjes, J., 2004. The role of grazing in structuring Southern Ocean pelagic ecosystems and biogeochemical cycles. Antarct. Sci. 16, 541–558. doi:10.1017/S0954102004002317

Smetacek, V.S., 1985. Role of sinking in diatom life-history cycles: ecological, evolutionary and geological significance. Mar. Biol. 84, 239–251. doi:10.1007/BF00392493

Steinberg, D.K., Goldthwait, S.A., Hansell, D.A., 2002. Zooplankton vertical migration and the active transport of dissolved organic and inorganic nitrogen in the Sargasso Sea. Deep Sea Res. Part Oceanogr. Res. Pap. 49, 1445–1461. doi:10.1016/S0967-0637(02)00037-7

Suzuki, H., Sasaki, H., Fukuchi, M., 2001. Short-term variability in the flux of rapidly sinking particles in the Antarctic marginal ice zone. Polar Biol. 24, 697–705. doi:10.1007/s003000100271

Suzuki, H., Sasaki, H., Fukuchi, M., 2003. Loss Processes of Sinking Fecal Pellets of Zooplankton in the Mesopelagic Layers of the Antarctic Marginal Ice Zone. J. Oceanogr. 59, 809–818. doi:10.1023/B:JOCE.0000009572.08048.0d

Takahashi, T., Sweeney, C., Hales, B., Chipman, D., Newberger, T., Goddard, J., Iannuzzi, R., Sutherland, S., 2012. The Changing Carbon Cycle in the Southern Ocean. Oceanography 25, 26–37. doi:10.5670/oceanog.2012.71

Takeda, S., 1998. Influence of iron availability on nutrient consumption ratio of diatoms in oceanic waters. Nature 393, 774–777. doi:10.1038/31674

Tarling, G.A., Ward, P., Atkinson, A., Collins, M.A., Murphy, E.J., 2012. DISCOVERY 2010: Spatial and temporal variability in a dynamic polar ecosystem. Deep Sea Res. Part II Top. Stud. Oceanogr. 59–60, 1–13. doi:10.1016/j.dsr2.2011.10.001

Taylor, S.R., McClennan, S.M., 1986. The continental crust: Its composition and evolution. Geol. J. 21, 85–86. doi:10.1002/gj.3350210116

Thomalla, S.J., Fauchereau, N., Swart, S., Monteiro, P.M.S., 2011. Regional scale characteristics of the seasonal cycle of chlorophyll in the Southern Ocean. Biogeosciences 8, 2849–2866. doi:10.5194/bg-8-2849-2011

Treppke, U.F., Lange, C.B., Wefer, G., 1996. Vertical fluxes of diatoms and silicoflagellates in the eastern equatorial Atlantic, and their contribution to the sedimentary record. Mar. Micropaleontol. 28, 73–96. doi:10.1016/0377-8398(95)00046-1

Uitz, J., Claustre, H., Griffiths, F.B., Ras, J., Garcia, N., Sandroni, V., 2009. A phytoplankton class-specific primary production model applied to the Kerguelen Islands region (Southern Ocean). Deep Sea Res. Part Oceanogr. Res. Pap. 56, 541–560. doi:10.1016/j.dsr.2008.11.006

Venables, H., Moore, C.M., 2010. Phytoplankton and light limitation in the Southern Ocean: Learning from high-nutrient, high-chlorophyll areas. J. Geophys. Res. Oceans 115, C02015. doi:10.1029/2009JC005361

Von Bodungen, B., Fischer, G., Nöthig, E.-M., Wefer, G., 1987. Sedimentation of krill faeces during spring development of phytoplankton in Bransfield Strait, Antarctica. Mitt Geol Paläont Inst Univ Hambg. SCOPEUNEP Sonderbd 62, 243–257.

Weber, T.S., Deutsch, C., 2010. Ocean nutrient ratios governed by plankton biogeography. Nature 467, 550–554. doi:10.1038/nature09403

Wefer, G., Fischer, G., 1991. Annual primary production and export flux in the Southern Ocean from sediment trap data. Mar. Chem., Biochemistry and circulation of water masses in the Southern Ocean International Symposium 35, 597–613. doi:10.1016/S0304-4203(09)90045-7

Wefer, G., Fischer, G., Füetterer, D., Gersonde, R., 1988. Seasonal particle flux in the Bransfield Strait, Antartica. Deep Sea Res. Part Oceanogr. Res. Pap. 35, 891–898. doi:10.1016/0198-0149(88)90066-0

Wefer, G.G., Fisher, D.K., Futterer, R., Gersonde, R., Honjo, S., Ostermann, D., 1990. Particle sedimentation and productivity in Antarctic waters of the Atlantic sector., in: Geological History of the Polar Oceans : Arctic versus Antarctic. Kluwer Academic Publishers, The Netherlands, pp. 363–379.

Westberry, T.K., Behrenfeld, M.J., Milligan, A.J., Doney, S.C., 2013. Retrospective satellite ocean color analysis of purposeful and natural ocean iron fertilization. Deep Sea Res. Part Oceanogr. Res. Pap. 73, 1–16. doi:10.1016/j.dsr.2012.11.010

Wilson, S., E., Ruhl, H.A., Smith Jr, K.L., 2013. Zooplankton fecal pellet flux in the abyssal northeast Pacific: A 15 year time-series study. Limnol. Oceanogr. 58, 881–892. doi:10.4319/lo.2013.58.3.0881

Wilson, S.E., Steinberg, D.K., Buesseler, K.O., 2008. Changes in fecal pellet characteristics with depth as indicators of zooplankton repackaging of particles in the mesopelagic zone of the subtropical and subarctic North Pacific Ocean. Deep Sea Res. Part II Top. Stud. Oceanogr. 55, 1636–1647. doi:10.1016/j.dsr2.2008.04.019

Wolff, E.W., Fischer, H., Fundel, F., Ruth, U., Twarloh, B., Littot, G.C., Mulvaney, R., Röthlisberger, R., de Angelis, M., Boutron, C.F., Hansson, M., Jonsell, U., Hutterli, M.A., Lambert, F., Kaufmann, P., Stauffer, B., Stocker, T.F., Steffensen, J.P., Bigler, M., Siggaard-Andersen, M.L., Udisti, R., Becagli, S., Castellano, E., Severi, M., Wagenbach, D., Barbante, C., Gabrielli, P., Gaspari, V., 2006. Southern Ocean sea-ice extent, productivity and iron flux over the past eight glacial cycles. Nature 440, 491–496. doi:10.1038/nature04614

Yoon, W., Kim, S., Han, K., 2001. Morphology and sinking velocities of fecal pellets of copepod, molluscan, euphausiid, and salp taxa in the northeastern tropical Atlantic. Mar. Biol. 139, 923–928. doi:10.1007/s002270100630

Zielinski, U., Gersonde, R., 1997. Diatom distribution in Southern Ocean surface sediments (Atlantic sector): Implications for paleoenvironmental reconstructions. Palaeogeogr. Palaeoclimatol. Palaeoecol. 129, 213–250. doi:10.1016/S0031-0182(96)00130-7

Table 1. Sediment trap cup collection dates, seasonal attribution, particulate organic carbon (POC) and nitrogen (PON) fluxes, biogenic and lithogenic silicon (BSi and LSi) fluxes and molar ratios. POC and PON data from Rembauville et al. (2014).

Cup	Cup opening date	Cup closing date	Collection time (days)	Season	Mass flux (mg m^{-2} d^{-1})	POC flux (mmol m^{-2} d^{-1})	PON flux (mmol m^{-2} d^{-1})	BSi Flux (mmol m^{-2} d^{-1})	LSi flux (µmol m^{-2} d^{-1})	% opal	POC:PON	BSi:POC
1	21/10/2011	04/11/2011	14	Spring	52.2	0.15	0.02	0.51	26.6	65.6	6.80	3.46
2	04/11/2011	18/11/2011	14	Spring	28.1	0.14	0.02	0.30	18.0	70.8	6.09	2.18
3	18/11/2011	02/12/2011	14	Spring	54.1	0.15	0.02	0.51	13.0	63.9	7.33	3.43
4	02/12/2011	12/12/2011	10	Summer	261.3	1.60	0.23	2.60	20.9	66.9	6.95	1.63
5	12/12/2011	22/12/2011	10	Summer	23.1	0.34	0.05	0.21	4.4	62.4	6.87	0.64
6	22/12/2011	01/01/2012	10	Summer	74.8	0.51	0.08	0.37	8.2	32.9	6.70	0.72
7	01/01/2012	11/01/2012	10	Summer	80.5	0.42	0.06	0.55	8.9	46.0	6.73	1.32
8	11/01/2012	25/01/2012	14	Summer	59.8	0.34	0.05	0.50	5.4	56.5	6.94	1.48
9	25/01/2012	08/02/2012	14	Summer	238.7	1.47	0.20	2.19	7.2	61.7	7.38	1.49
10	08/02/2012	22/02/2012	14	Summer	75.8	0.55	0.08	0.72	6.1	64.2	6.97	1.32
11	22/02/2012	31/05/2012	99	Autumn	24.4	0.27	0.03	0.08	1.5	21.5	8.09	0.29
12	31/05/2012	07/09/2012	99	Winter	5.1	0.04	0.01	0.03	2.2	35.0	6.06	0.66
Annual export (mmol m^{-2} y^{-1})						98.2	13.6	114	1.85			

Table 2. *Chaetoceros* resting spores (CRS) and *Thalassiosira antarctica* resting spores (TRS) measurement and biomass data from station A3 sediment trap covering cups #4 (December 2011) to #11 (April 2012). For each variable, the range and the mean value (bold italic) is reported.

Spore type	Number measured	Pervalvar axis (µm)	Apical axis (µm)	Shape *	Cell volume (μm^3)	Volume/Carbon relationship	Cell carbon content (pmolC $cell^{-1}$)	Cell carbon content (pgC $cell^{-1}$)
CRS	63	3.1 – 8.5 ***6***	7.2 - 17.4 ***12.1***	Cylinder + two cones	116.9 – 1415 ***483***	0.039 pmolC μm^{-3} #	5 – 55 ***19***	55 – 662 ***227***
TRS	57	10.2 – 26 ***20.8***	25.6 – 35.3 ***32.6***	Cylinder + two half sphere	14035 – 48477 ***35502***	$C = 10^{(0.811 \log10(V)) - 0.541)}$ §	56 - 153 ***119***	672 - 1839 ***1428***

* As defined in Hillebrand et al., (1999)

Data representative of *Chaetoceros pseudocurvisetus* resting spore (Kuwata et al. 1993)

§ Equation from Menden-Deuer and Lessard, (2000), where C is the carbon content (pg C) and V is the cell volume (μm^3)

Table 3. Faecal pellet measurement and biomass estimations from Station A3 sediment trap. For each variable, the range and the mean value (bold italic) are reported.

Faecal pellet shape	Number measured	Major axis (µm) (a)	Minor axis (µm) (b)	Volume equation	Volume (μm^3)	Volume/carbon relationship	Faecal pellet carbon content (µmolC $pellet^{-1}$)	Faecal pellet carbon content (µgC $pellet^{-1}$)
Spherical	4041	11 - 1069 ***150***		$4/3\ \pi\ (a/2)^3$	697 - 6.39×10^8 ***1.77×10^6***		2.09×10^{-6} – 1.91 ***$5.3\ 10^{-3}$***	2.51×10^{-5} - 23 ***0.06***
Ovoid	2047	85 - 1132 ***314***	10-802 ***154***	$4/3\ \pi\ (a/2)\ (b/2)^2$	4.45×10^3 - 3.81×10^8 ***3.90×10^6***	0.036 mgC mm^{-3} *	1.34×10^{-5} – 1.14 ***11.7×10^{-3}***	1.60×10^{-4} – 13.72 ***0.14***
Cylindrical	1338	106 - 6152 ***981***	14-547 ***136***	$\pi\ (b/2)^2\ a$	1.63×10^4 – 1.45×10^9 ***1.43×10^7***		4.89×10^{-4} – 4.35 ***0.04***	5.87×10^{-4} - 52 ***0.51***
Ellipsoid	54	301 - 3893 ***1329***	51-1051 ***413***	$4/3\ \pi\ (a/2)\ (b/2)^2$	4.10×10^5 – 2.25×10^9 1.19×10^8		1.2×10^{-3} – 6.75 ***0.36***	0.01 - 81 ***4.28***
Tabular	29					Constant, 119 µgC $pellet^{-1}$ #	9.92	119

* Gonzalez and Smetacek, (1994)

Wilson et al. (2013)

Table 4. Full diatoms cells flux (10^6 m^{-2} d^{-1}) from the station A3 sediment trap. Full cells of *Chaetoceros Hyalochaete* spp. were only found as resting spores.

Species – taxa group	Cup number 1	2	3	4	5	6	7	8	9	10	11	12	Contribution to annual flux (%)
***Asteromphalus* spp.**	0	0.01	0	0.03	0	0	0	0	0.12	0	0	0	0.1
***Chaetoceros atlanticus* Cleve**	0	0	0	0	0	0	0	0	0.07	0	0	0	0.0
***Chaetoceros atlanticus* f. *bulbosus* Ehrenberg**	0	0	0	0	0	0	0	0	0	0	0	0	0.0
***Chaetoceros decipiens* Cleve**	0	0	0.02	0	0	0	0	0	0.07	0	0	0	0.0
***Chaetoceros dichaeta* Ehrenberg**	0	0	0	0.07	0	0	0	0	0.26	0	0	0	0.1
***Chaetoceros Hyalochaete* spp.**	0.70	0	1.95	39.92	7.42	23.04	14.37	15.88	78.29	20.24	0.68	0	80.2
***Corethron inerme* Karsten**	0	0	0	0	0	0	0	0	0.23	0	0	0	0.1
***Corethron pennatum* Grunow**	0	0	0	0	0	0	0	0	0	0	0	0	0.0
***Dactyliosolen antarcticus* Castracane**	0	0	0	0.05	0	0	0	0	0.02	0	0	0	0.0
***Eucampia antarctica* var. *antarctica* (Castracane) Mangin**	0.08	0.03	0.06	0.19	0.08	0.36	0.19	0.65	1.03	0.45	0.08	0.01	1.6
***Fragilariopsis kerguelensis* (O'Meara) Hustedt**	0.88	1.06	0	1.93	0.40	0.13	0.21	0.12	1.40	0	0	0	2.4
***Fragilariopsis separanda/rhombica* group**	0.02	0.16	0	0.68	0.05	0.20	0.13	0.07	1.47	0	0	0	1.1
***Guinardia cylindrus* (Cleve) Hasle**	0	0	0	0	0	0	0	0	0.07	0	0	0	0.0
***Leptocylindrus* sp.**	0	0	0	0.03	0	0	0	0	0	0	0	0	0.0
***Membraneis* spp.**	0.04	0.01	0	0.19	0	0	0.02	0.02	0.02	0	0	0	0.1
***Navicula* spp.**	0	0	0.04	0.64	0	0	0	0.29	0.58	0	0	0	0.6
***Odontella weissflogii* (Grunow) Grunow**	0	0	0	0.08	0	0	0	0	0.05	0	0	0	0.0
***Pleurosigma* spp.**	0.01	0	0	0.22	0.02	0.02	0	0.03	0.96	0.04	0	0	0.5
***Proboscia alata* (Brightwell) Sundröm**	0	0	0	0	0	0	0	0	0.09	0	0	0	0.0
***Proboscia inermis* (Castracane) Jordan & Ligowski**	0	0	0	0.03	0	0	0	0	0.33	0	0	0	0.2
***Proboscia truncata* (Karsten) Nöthig & Logowski**	0	0	0	0	0	0	0	0	0	0	0	0	0.0
***Pseudo-nitzschia* spp.**	0.26	0.02	0.21	1.81	0.08	0.45	1.85	1.56	7.08	0.36	0.02	0	5.6
***Rhizosolenia antennata/styliformis* group**	0	0	0	0	0	0	0	0	0.05	0	0	0	0.0
***Rhizosolenia chunii* Karsten**	0	0	0	0	0.05	0	0	0.03	0.07	0	0	0	0.1
***Rhizosolenia crassa* Schimper in Karsten**	0	0	0	0	0	0	0	0	0	0	0	0	0.0
***Rhizosolenia simplex* Karsten**	0	0	0	0	0	0	0	0	0.07	0	0	0	0.0
***Thalassionema nitzschioides* spp. Pergallo & Pergallo**	1.45	1.48	0.20	4.65	0.28	0.14	0.34	0.72	0.89	0.14	0.05	0.01	4.0
***Thalassiosira lentiginosa* (Janisch) Fryxell**	0.01	0	0	0	0	0	0	0	0	0	0	0	0.0
***Thalassiosira* spp.**	0	0.05	0	0.05	0	0	0	0	0.12	0.05	0	0	0.1
***Thalassiosira antarctica* resting spore (TRS) Comber**	0.04	0	2.19	2.65	0.17	0.14	0.13	0.14	0.12	0	0.01	0	2.1

***Thalassiothrix antarctica* Schimper ex Karsten**	0	0	0	0.02	0.05	0.04	0.34	0.14	0.70	0	0	0	0.5
Small centrics (<20 µm)	0.05	0	0	0.41	0	0	0	0	0.19	0.18	0	0	0.3
Large centrics (>20 µm)	0	0	0.05	0.08	0	0	0	0	0.05	0	0	0	0.1
Total full cells	35.39	28.20	47.18	537.38	85.85	245.20	175.89	196.56	943.88	214.65	8.46	0.22	

1394

1395

1396 **Table 5.** Empty diatoms cells flux (10^6 m^{-2} d^{-1}) from the station A3 sediment trap.

1397

Species – taxa group / Cup Number	Empty Cells 1	2	3	4	5	6	7	8	9	10	11	12	Contribution to annual flux (%)
***Asteromphalus* spp.**	0.02	0.02	0.09	0.08	0	0.05	0	0.03	0.05	0	0	0	0.3
***Chaetoceros atlanticus* Cleve**	0	0	0	0	0	0	0	0	0	0	0	0	0.0
***Chaetoceros atlanticus* f. *bulbosus* Ehrenberg**	0.01	0	0	0	0	0	0	0.02	0	0.02	0	0	0.0
***Chaetoceros decipiens* Cleve**	0	0	0.02	0.24	0	0	0	0	0	0	0	0	0.2
***Chaetoceros dichaeta* Ehrenberg**	0	0	0.06	0.07	0	0	0	0	0.05	0	0.01	0	0.2
***Chaetoceros Hyalochaete* spp.**	0	0	0.45	38.19	0	0	0	0.60	18.23	0.18	0	0	41.2
***Corethron inerme* Karsten**	0.01	0.01	0.04	0	0	0.02	0	0	0.23	0.31	0.06	0	0.9
***Corethron pennatum* Grunow**	0	0	0.02	0	0	0	0	0.02	0	0	0.01	0	0.1
***Dactyliosolen antarcticus* Castracane**	0	0	0	0.05	0	0	0	0.07	0.02	0.05	0	0	0.2
***Eucampia antarctica* var. *antarctica* (Castracane) Mangin**	0	0	0.04	0.25	0.06	0.05	0.06	0.09	0.28	0.11	0.04	0	1.0
***Fragilariopsis kerguelensis* (O'Meara) Hustedt**	2.25	0.46	0.84	1.02	0.26	0.63	0.88	1.17	1.17	1.45	0.16	0.03	9.4
***Fragilariopsis separanda/rhombica* group**	0.19	0.17	0.18	0.53	0.14	0.52	0.32	0.87	0.82	1.23	0.15	0	5.0
***Guinardia cylindrus* (Cleve) Hasle**	0	0	0	0	0	0	0	0	0	0	0	0	0.0
***Leptocylindrus* sp.**	0	0	0	0	0	0	0	0	0	0	0	0	0.0
***Membraneis* spp.**	0	0	0.02	0.05	0.02	0.04	0.02	0.07	0.14	0.07	0.01	0	0.4
***Navicula* spp.**	0	0	0.13	0.36	0	0	0	0.12	0.12	0	0	0	0.5
***Odontella weissflogii* (Grunow) Grunow**	0	0	0.02	0.10	0	0	0	0.02	0	0.02	0	0	0.1
***Pleurosigma* spp.**	0.18	0.06	0.08	0.41	0.08	0	0.09	0.12	0.93	0.38	0.03	0	2.1
***Proboscia alata* (Brightwell) Sundröm**	0	0	0	0	0	0	0	0.03	0.05	0.34	0.01	0	0.5
***Proboscia inermis* (Castracane) Jordan & Ligowski**	0	0	0.01	0.08	0	0	0	0.03	0.05	0.13	0.01	0	0.3
***Proboscia truncata* (Karsten) Nöthig & Logowski**	0	0	0.02	0	0	0	0	0	0	0.02	0	0	0.0
***Pseudo-nitzschia* spp.**	0.59	0	0.12	0.59	0.09	0.04	0.99	0.75	5.26	0.34	0.02	0	7.4
***Rhizosolenia antennata/styliformis* group**	0	0	0	0	0	0	0	0.02	0.02	0.13	0	0	0.2
***Rhizosolenia chunii* Karsten**	0	0	0	0.03	0	0	0	0.02	0.02	0.20	0.02	0	0.4
***Rhizosolenia crassa* Schimper in Karsten**	0	0	0	0	0	0	0	0	0	0.04	0	0	0.0
***Rhizosolenia simplex* Karsten**	0	0	0	0	0	0	0	0.02	0	0	0	0	0.0
***Thalassionema nitzschioides* spp. Pergallo & Pergallo**	4.33	1.97	5.39	2.07	0.19	0.09	0.47	0.12	0.72	0.18	0.03	0.01	13.2
***Thalassiosira lentiginosa* (Janisch) Fryxell**	0.25	0.06	0.10	0	0	0	0	0	0	0	0	0	0.4
***Thalassiosira* spp.**	0.02	0.06	0.01	0	0	0	0	0	0	0	0	0	0.1
***Thalassiosira antarctica* resting spore (TRS) Comber**	0	0	0	0	0	0	0	0	0	0	0	0	0.0

***Thalassiothrix antarctica* Schimper ex Karsten**	0	0	0	0	0	0.02	0	0	0	0.04	0	0	0.0
Small centrics (<20 µm)	0.48	0.44	2.96	16.87	0.28	0.13	0.17	0.24	0.65	0.20	0.03	0.02	15.7
Large centrics (>20 µm)	0	0.03	0.01	0.20	0	0	0	0	0.16	0.04	0	0	0.3
Total empty cells	8.34	3.28	10.57	61.20	1.12	1.59	3.01	4.43	28.98	5.46	0.59	0.07	

1398

1399

Table 6. Total faecal pellet (FP) flux, total faecal pellet carbon flux, median volume and carbon flux partitioned among faecal pellets types from station A3 sediment trap. Contribution to numerical faecal pellet flux is provided in normal text whereas the contribution to faecal pellet carbon flux is reported in bold italic.

				Contribution (%)				
Cup	**Total FP flux (nb m^{-2} d^{-1}) × 10^3**	**Total FP carbon flux (mmol m^{-2} d^{-1})**	**Median volume (10^6 µm^3)**	**Spherical**	**Ovoid**	**Cylindrical**	**Ellipsoid**	**Tabular**
1	1.39	0.02	2.07	53.3	19.7	27.0	0.0	0.0
				36.8	***18.6***	***44.6***	***0.0***	***0.0***
2	1.75	0.04	3.55	36.5	29.7	33.9	0.0	0.0
				22.4	***21.3***	***56.3***	***0.0***	***0.0***
3	0.72	<0.01	0.95	62.7	37.3	0.0	0.0	0.0
				54.5	***45.5***	***0.0***	***0.0***	***0.0***
4	21.81	0.48	1.91	76.4	22.8	0.8	0.0	0.0
				83.1	***15.3***	***1.6***	***0.0***	***0.0***
5	5.10	0.12	3.71	26.6	35.0	38.3	0.1	0.0
				13.8	***18.3***	***67.4***	***0.5***	***0.0***
6	2.69	0.15	5.67	28.8	33.1	37.9	0.0	0.2
				4.6	***10.9***	***43.1***	***0.0***	***41.3***
7	2.46	0.12	6.71	15.6	45.5	37.1	1.8	0.0
				2.5	***16.1***	***56.0***	***25.3***	***0.0***
8	2.06	0.20	6.18	37.6	15.5	44.2	2.2	0.4
				1.9	***2.1***	***34.6***	***15.8***	***45.5***
9	1.36	0.09	3.59	40.4	20.5	35.4	3.7	0.0
				2.8	***4.9***	***27.9***	***64.4***	***0.0***
10	1.22	0.03	2.34	56.0	22.4	21.3	0.4	0.0
				17.7	***9.1***	***69.9***	***3.3***	***0.0***
11	0.27	0.13	2.10	38.9	30.8	20.3	5.7	4.3
				0.4	***0.7***	***2.5***	***3.9***	***92.6***
12	0.14	0.06	2.41	18.4	57.6	20.3	0.0	3.7
				0.4	***2.6***	***5.3***	***0.0***	***91.8***
Annually integrated contribution to faecal pellet flux				53.8	27.3	17.8	0.7	0.4
				17.9	***6.6***	***17.3***	***7.7***	***50.4***

Table 7. Measured and calculated POC fluxes, and POC flux partitioning among the major identified ecological vectors of carbon exported out of the mixed layer at station A3. Measured total POC flux from Rembauville et al. (2014). CRS: *Chaetoceros Hyalocahete* resting spores, TRS: *Thalassiosira antarctica* resting spore.

			Contribution to calculated POC flux (%)								
Cup	**Measured POC flux (mmol m^{-2} d^{-1})**	**Calculated POC flux (mmol m^{-2} d^{-1})**	**CRS**	**TRS**	**Other diatoms**	**Spherical faecal pellet**	**Ovoid faecal pellet**	**Cylindrical faecal pellet**	**Ellipsoid faecal pellet**	**Tabular faecal pellet**	**Total faecal pellet**
1	0.15	0.05	25.3	8.1	38.6	10.3	5.2	12.5	0.0	0.0	28.0
2	0.14	0.06	0.0	0.0	35.4	14.5	13.7	36.4	0.0	0.0	64.6
3	0.15	0.31	12.1	85.1	1.4	0.8	0.6	0.0	0.0	0.0	1.4
4	1.60	1.62	46.8	19.4	3.9	24.8	4.6	0.5	0.0	0.0	29.8
5	0.34	0.29	48.0	6.9	3.3	5.8	7.7	28.2	0.2	0.0	41.8
6	0.51	0.63	69.7	2.7	3.2	1.1	2.7	10.5	0.0	10.1	24.4
7	0.42	0.43	63.1	3.5	5.8	0.7	4.4	15.4	7.0	0.0	27.5
8	0.34	0.56	54.4	2.9	6.8	0.7	0.8	12.4	5.7	16.3	35.9
9	1.47	1.71	86.8	0.8	7.2	0.1	0.3	1.4	3.3	0.0	5.2
10	0.55	0.44	88.1	0.0	4.3	1.4	0.7	5.4	0.3	0.0	7.7
11	0.27	0.14	9.1	1.2	2.2	0.3	0.6	2.2	3.4	81.0	87.5
12	0.04	0.06	0.0	0.0	0.5	0.4	2.6	5.2	0.0	91.3	99.5
Contribution to annual calculated POC flux (%)			52.1	8.6	5.0	5.1	2.0	5.2	2.2	19.8	34.3

Figures captions.

Figure 1. a) Time series of the surface chlorophyll *a* concentration averaged in a 100 km radius around the trap location. The black line represents the climatology calculated for the period 1997/2013, whilst the green line corresponds to the sediment trap deployment period (2011/2012). b) POC fluxes (grey bars) and C/N molar ratio (red line) of the exported material, c) BSi flux (light blue bars) and BSi:POC ratio (blue line). Errorbars are standard deviation on triplicates.

Figure 2. a) Total diatom cells fluxes (bars, left axis) and total empty:full cells ratio (blue line, right axis). b) to h) Fluxes of diatom cells from selected species identified as major contributors to diatom fluxes (>1 % of total diatom fluxes). In b), full cells are *Chaetoceros Hyalochaete* resting spores and empty cells are the vegetative stage. Full cell fluxes are represented by grey bars whereas empty cell fluxes are represented by white bars

Figure 3. Factorial map constituted by the first two axes of the correspondence analysis performed on the full and empty diatom cell fluxes. Red squares are cup projections with cup numbers specified, blue circles are full cell projections, white circles are empty cell projections. The size of the markers is proportional to their representation quality in this factorial map.

Figure 4. Annual ratio of empty to full cells for species observed as both forms. The dashed lines are the 0.5 and 2 ratio values. *Chaetoceros Hyalochaete* spp. full cells were only observed as resting spores.

Figure 5. a) Faecal pellet numerical fluxes partitioned among faecal pellet types, b) boxplot of faecal pellet volume. On each box, the central mark is the median, the edges of the box are the first and third quartiles, the whiskers extend to the most extreme data points comprised in 1.5 times the interquartile distance. c) faecal pellet carbon fluxes partitioned between the five

faecal pellet types. The two arrows represent the two strong POC export events (cup #4 and #9, December 2011 and end January 2012, respectively).

Figure 6. Heatmap representation of β correlation coefficients between the biological variables (empty and full-cell diatom and faecal pellet type fluxes) and the chemical variables (POC, PON, BSi, POC:PON and BSi:POC) resulting from the partial least square regression. Blue circles represent full diatom cells, white circles are empty diatom cells. Brown circles represent the faecal pellet type fluxes. The alphabetical labels within the symbols are used to identify the variable projections shown in Fig. 7. CRS: *Chaetoceros Hyalochaete* resting spores, TRS: *Thalassiosira antarctica* resting spores.

Figure 7. Projection of the cups (red squares) the biological factors (circles) and the chemical factors (green diamonds) in the first two latent vectors of the partial least square regression. Circled labels refer to the full and empty species listed in Fig. 6.

Figure 8. a) Grey bars in the background are measured POC fluxes, colored bars in the foreground are calculated POC fluxes partitioned among the main ecological vectors identified. b) Regression ($r^2 = 0.72$) between the measured and calculated POC fluxes. The correlation is highly significant (Spearman rank correlation, $n = 36$, $\rho = 0.84$, $p < 0.001$). Error bars were generated by increasing/decreasing the carbon/volume conversion factors by 50 %. Black dashed line is the 1:1 relation, red line is the regression line, red dashed lines denotes the 99 % confidence interval. CRS: *Chaetoceros Hyalochaete* resting spores, TRS: *Thalassiosira antarctica* resting spores.

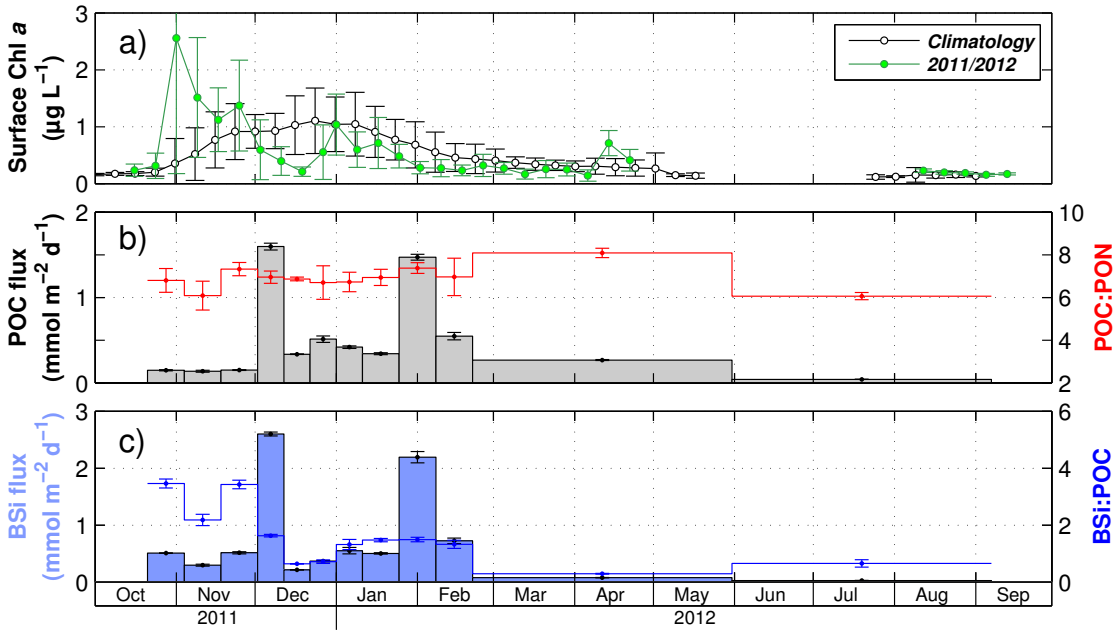

Figure 1.

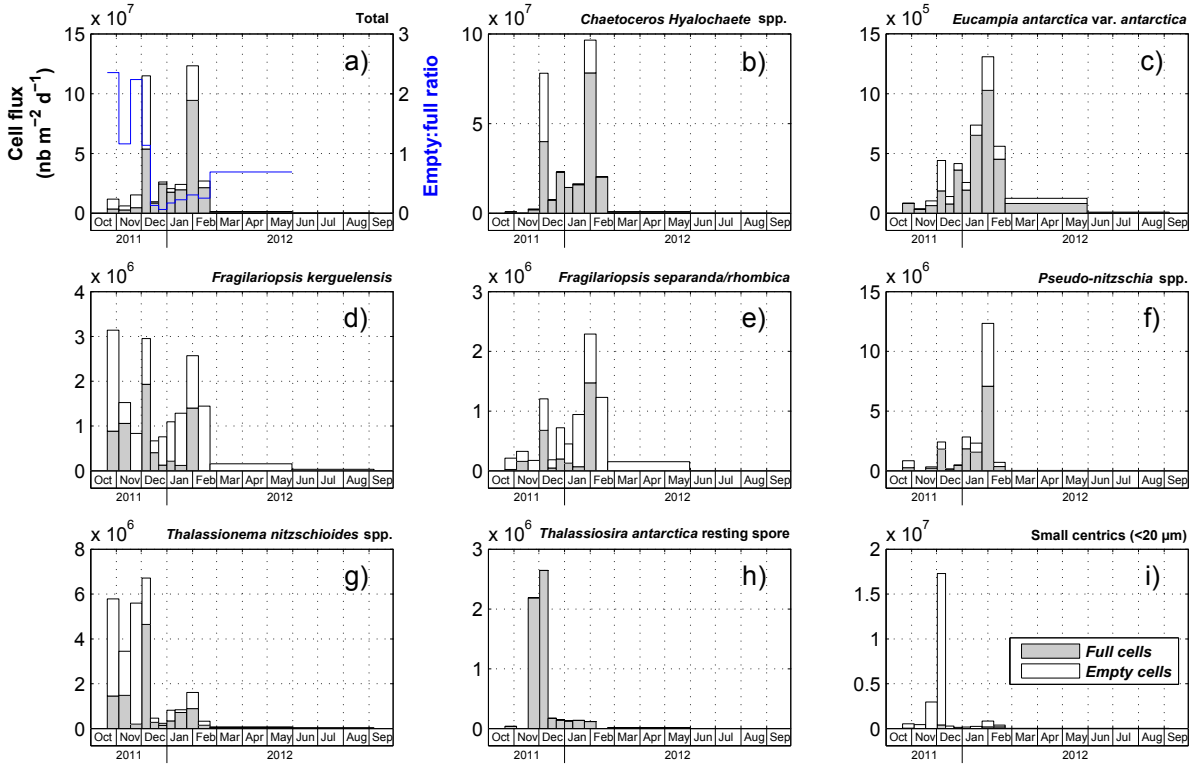

Figure 2.

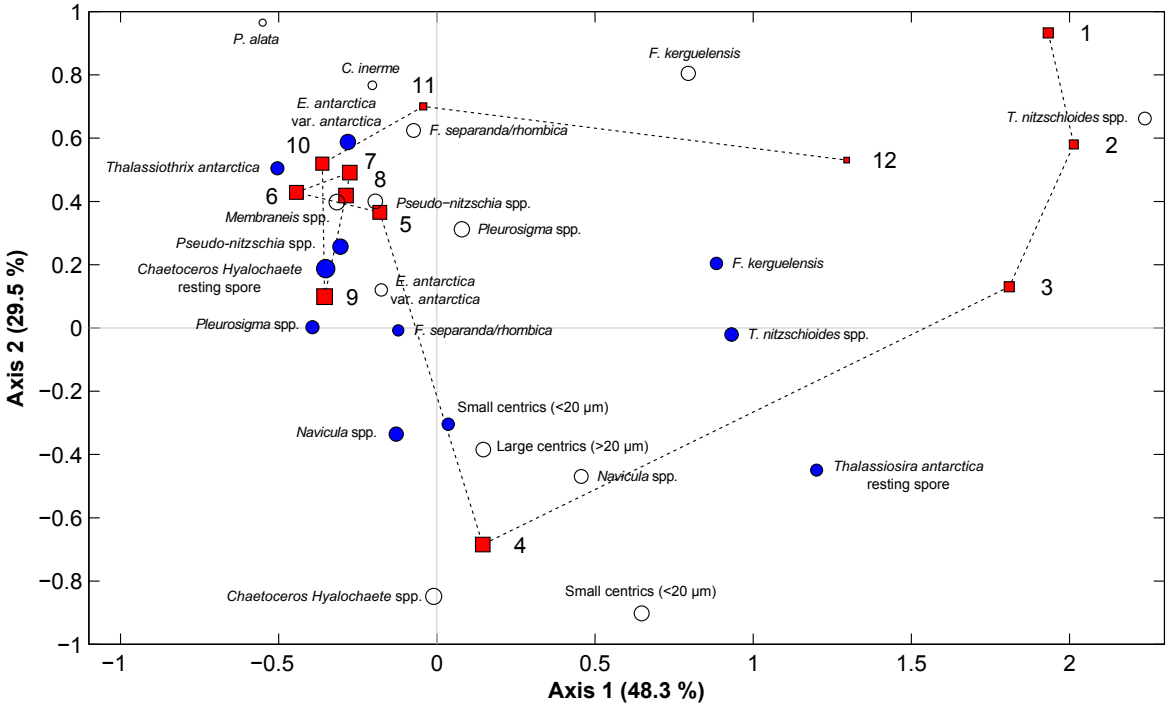

Figure 3.

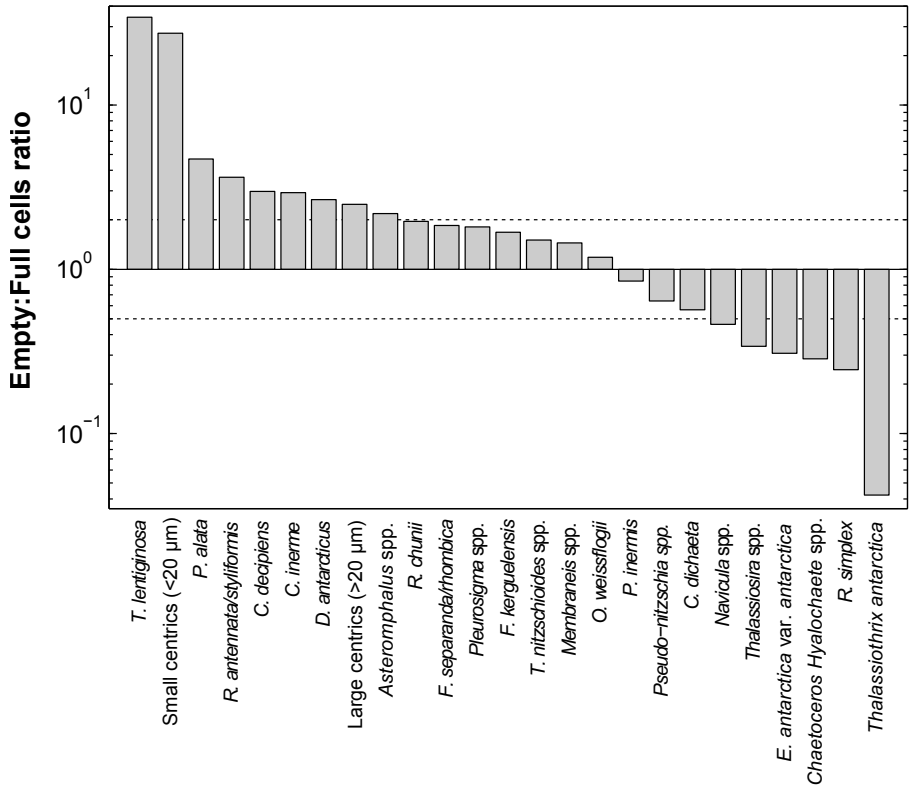

Figure 4.

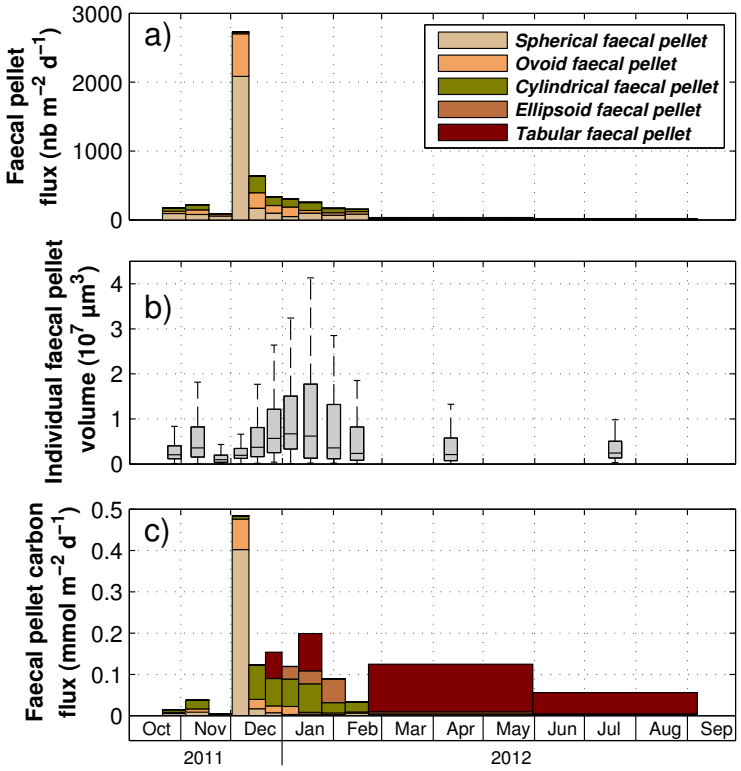

Figure 5.

		POC	PON	BSi	POC:PON	BSi:POC
ⓐ	CRS	0.07	0.07	0.06	0.02	−0.04
ⓑ	*E. antarctica*	0.05	0.05	0.03	0.02	−0.04
ⓒ	*F. kerguelensis*	0.05	0.05	0.07	0	0.07
ⓓ	*F. separanda/rhombica*	0.06	0.06	0.06	0.02	−0.01
ⓔ	*Navicula* spp.	0.07	0.07	0.07	0.02	0
ⓕ	*Pleurosigma* spp.	0.06	0.06	0.05	0.02	−0.01
ⓖ	*Pseudo−nitzschia* spp.	0.06	0.05	0.05	0.02	−0.01
ⓗ	*T. nitzschioides* spp.	0.04	0.04	0.06	0	0.07
ⓘ	TRS	0.03	0.03	0.05	−0.01	0.1
ⓙ	*Thalassiothrix antarctica*	0.04	0.04	0.03	0.01	−0.03
ⓚ	Small centrics (<20 µm)	0.06	0.06	0.07	0.01	0.01
ⓐ	*Chaetoceros Hyalochaete* spp.	0.07	0.07	0.07	0.02	0
ⓑ	*C. inerme*	0.03	0.03	0.02	0.01	−0.03
ⓒ	*E. antarctica*	0.08	0.07	0.06	0.02	−0.04
ⓓ	*F. kerguelensis*	0	0.01	0.05	−0.02	0.17
ⓔ	*F. separanda/rhombica*	0.04	0.04	0.03	0.01	−0.03
ⓕ	*Membraneis* spp.	0.06	0.06	0.05	0.02	−0.04
ⓖ	*Navicula* spp.	0.05	0.05	0.06	0.01	0.05
ⓗ	*Pleurosigma* spp.	0.06	0.06	0.06	0.01	0.01
ⓘ	*P. alata*	0.01	0.01	0	0.01	−0.03
ⓙ	*Pseudo−nitzschia* spp.	0.05	0.05	0.05	0.01	0
ⓚ	*T. nitzschioides* spp.	−0.03	−0.02	0.04	−0.04	0.24
ⓛ	*T. lentiginosa*	−0.04	−0.04	0.02	−0.04	0.22
ⓜ	Small centrics (<20 µm)	0.05	0.05	0.06	0.01	0.04
ⓝ	Large centrics (>20 µm)	0.07	0.07	0.07	0.02	0.01
Ⓢ	Spherical faecal pellet	0.05	0.05	0.05	0.01	0.01
Ⓞ	Ovoid faecal pellet	0.05	0.05	0.04	0.01	−0.02
Ⓒ	Cylindrical faecal pellet	0	0	−0.02	0.01	−0.08
Ⓔ	Ellipsoid faecal pellet	0.03	0.03	0.01	0.01	−0.06
Ⓣ	Tabular faecal pellet	−0.01	−0.01	−0.05	0.02	−0.15

Figure 6.

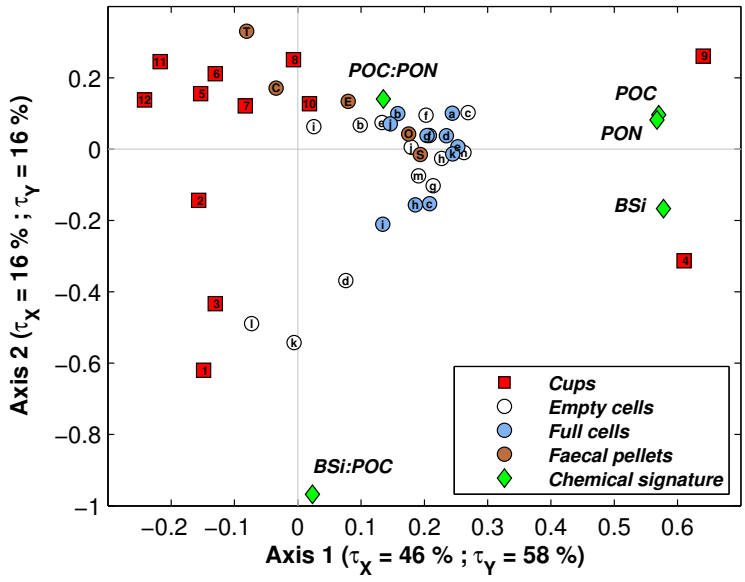

Figure 7.

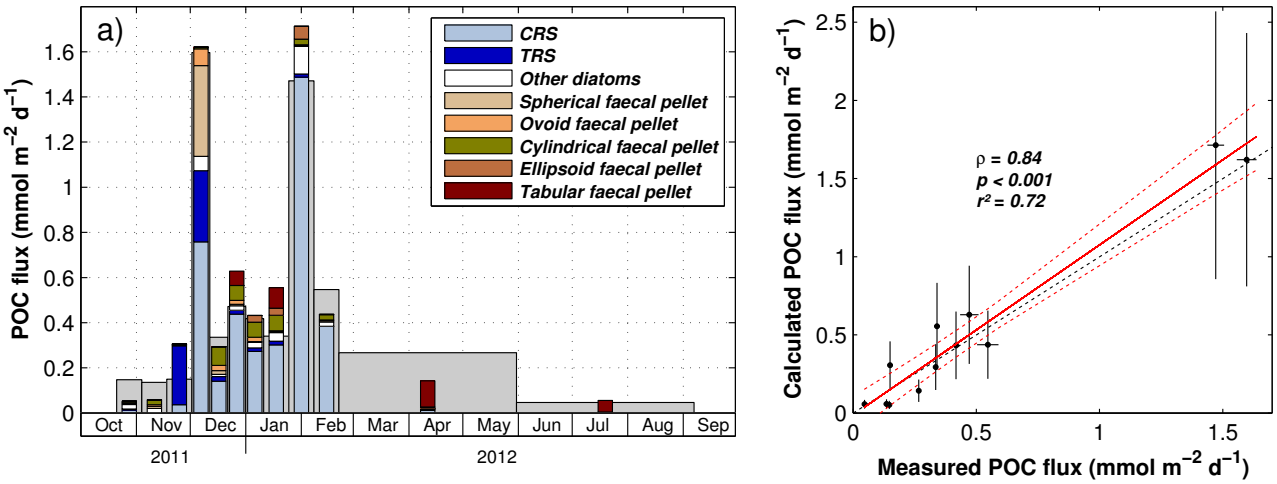

Figure 8.